J. Fluid Mech. (2025), *vol*. 1005, A1, doi:10.1017/jfm.2024.1062

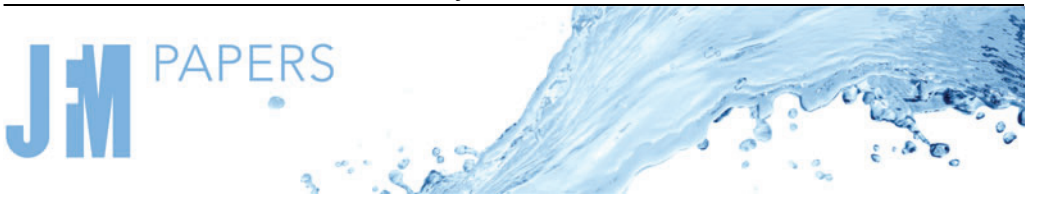

Roles of interfacial-exchange kinetics and interfacial-charge mobility on fluid-sphere electrophoresis

Reghan J. Hill†

Department of Chemical Engineering, McGill University, Montreal, Quebec, Canada

(Received 6 May 2024; revised 25 August 2024; accepted 25 October 2024)

Electrophoretic characterization of nano- and micro-metre scaled bubbles and drops is increasingly important in environmental and health sciences. Despite more than a hundred years of study, the interpretation of bubble electrophoresis data remains an unresolved fundamental problem that bridges fluid mechanics and interfacial science. This paper examines, from a theoretical perspective, how the electrophoretic mobility of small drops and bubbles responds to the interfacial kinetic-exchange rate and interfacial-charge mobility: factors that have been largely overlooked, but which provide new insights on the interpretation of ζ-potentials, which are routinely used to assess surface charge density. A variety of outcomes are demonstrated, each reflecting subtle balances of hydrodynamic and electrical forces, modulated by interfacial thermodynamics and transport. Among the findings is that irreversibly bound charge with low interfacial mobility furnishes rigid-sphere behaviour; whereas interfacial charge with high mobility produces the characteristically high electrophoretic mobilities of non-conducting, uniformly charged fluid spheres. Outcomes are more complex when drops and bubbles have interfacial charge that seeks local equilibrium with the immediately adjacent electrolyte. For example, the present model shows that interfacial-charge mobility regularizes the singular behaviour predicted by theories for fluid spheres bearing high, perfectly uniform surface charge.

Key words: bubbles, drops, electrokinetic flows

1. Introduction

Small drops and bubbles are often the microstructural foundation of dispersions, emulsions and foams, and are of increasing significance in a broad range of environmental and health related fields. Lyu *et al.* (2019) highlight nanobubble technologies being harnessed for

† Email address for correspondence: reghan.hill@mcgill.ca

biomedical applications and tackling environmental issues. Among these, nanobubbles with size $\sim$100 nm have been demonstrated as effective in preventing surface fouling, and for cleaning already fouled surfaces (Zhu *et al.* 2016). Bubbles in the environment have recently been identified as responsible for an unexpectedly large portion of the air–sea flux of oxygen, suggesting that oxygen levels in the deep ocean may be much more sensitive to climate change than previously thought (Atamanchuk *et al.* 2020). This seems to reflect a small size (low buoyancy) and stability to coalescence: factors that may also play into the transport and fate of droplet-based environmental pollutants (Adams, Brown & Hodson 2020). In biomedicine, the small size of 'acoustic nanodrops' (e.g. perfluorocarbons) avoids their detection by the immune system, enabling on-demand vaporization for detection and manipulation with ultrasound (Borden *et al.* 2020).

Explanations of fluid-sphere stability to coalescence (Ho *et al.* 2022) and of nanobubble existence (Zhang, Guo & Zhang 2020) are grounded on the interfacial-charge density, which is typically ascertained from the ζ-potential (routinely used to assess surface charge density) furnished by electrophoresis experiments. However, such experiments are invariably interpreted as if bubbles and drops are rigid spheres. Although steady electrophoresis is nowadays routinely performed using commercially available electrophoretic light-scattering instruments, interpreting the electrophoretic mobility is complicated by internal and external fluid dynamics, and an interface that permits interfacial exchange and lateral transport of charged and uncharged surface-active molecules.

It is noted here that interfacial-charge mobility and kinetic exchange have been long recognized as pertinent to the electrophoretic mobility of rigid colloids, as exemplified by the dynamic Stern-layer model of Zukoski & Saville (1986). However, few studies have acknowledged these physics for fluid spheres, which is surprising given that these mechanisms should be even more important for fluid–fluid interfaces. Such interfacial physics were included in the fluid-sphere electrophoresis model of Baygents & Saville (1991), but their results focussed on examples with vanishing surface diffusivity and local equilibrium with the immediately adjacent electrolyte. It is not clear that these extremes are justified from a physical perspective, and so the consequences of relaxing these are known. Interfacial transport mechanisms were included in the dynamic mobility of fluid spheres by Hill & Afuwape (2020) and Hill (2020), but these interpreted the dynamic mobility spectra of emulsion drops from electrokinetic-sonic-amplitude experiments (in the megahertz frequency range), not the steady mobilities furnished by ubiquitous electrophoretic light-scattering instruments. There also remains the challenge of solving the equations (continuum conservation relationships) for two bulk phases and an interface.

It is customary for experimentalists to report fluid-sphere electrophoretic mobilities as ζ-potentials furnished by Henry's theory, which is for rigid/solid spheres bearing low surface potential (Russel, Saville & Showalter 1989); see Yang *et al.* (2001) and Takahashi (2005) for contemporary examples in the context of microbubbles; Ushikuboa *et al.* (2010), Nirmalkar, Pacek & Barigou (2018) and Jin *et al.* (2019) in the context of nanobubbles; and Pullanchery *et al.* (2020) in the context of nanodrops. Although convenient, this practice risks misinterpreting the ζ-potential in terms of the underlying surface charge (Hill 2020; Hill & Afuwape 2020). Note that, in the context of fluid spheres, the ζ-potential is adopted to identify the equilibrium electrostatic potential at the fluid–fluid interface, not necessarily an apparent or electrokinetic potential at a 'slipping plane'.

The pioneering fluid-sphere theory of Booth (1951) furnishes a convenient formula for small ζ-potentials (Debye–Hückel regime), but is seldom adopted to interpret experiments or directly test other theories and computations. Possible reasons for this will be elucidated

in the present study. Booth asserts a drop interface as maintaining a uniform charge density, but a mechanistic justification for this is not clear. For example, Baygents & Saville (1991) concluded consistency with Booth's theory (for non-ion-conducting fluid spheres), but, recall, this was achieved by setting the interfacial-charge mobility to nil and assuming local equilibrium between the interface and immediately adjacent electrolyte.

Other theoretical studies have extended Booth's theory with various embellishments, albeit for interfaces that bear perfectly uniform charge. For example, Mahapatra, Ohshima & Gopmandal (2022) addressed the dielectric contrast (ϵ_i/ϵ_o being the ratio of internal and external dielectric permittivities for non-ion-conducting fluid spheres), providing analytical formulas for low ζ-potentials and arbitrary κa (sphere radius a scaled with the Debye length κ^{-1}). A mobility that varies with dielectric permittivity contrast runs counter to the assertion of Baygents & Saville (1991) that the mobility is independent of the interior dielectric permittivity, as proved by O'Brien & White (1978) for rigid spheres. Note that Mahapatra *et al.* also allowed for hydrodynamic slip at the fluid–fluid interface, advancing closely related studies for uniform surface charge (Wu *et al.* 2021; Tsai *et al.* 2022; Tseng *et al.* 2023).

Despite more than a hundred years of experimental and theoretical investigation, there is no satisfactory interpretation of pioneering electrophoresis experiments conducted on air bubbles in water by Alty (1924) or others that follow, e.g. Whybrew, Kinzer & Gunn (1952), Usui, Sasaki & Matsukawa (1981) and Kelsall *et al.* (1996). According to Schnitzer, Frankel & Yariv (2013, 2014), the weak-field linearization underlying Booth's theory, and therefore Baygents & Saville (1991) and many others (including the present work), limits the particle size and electric-field strength for which the linearization is valid.

For large bubbles ($\kappa a \gg 1$) having a low viscosity ($\eta_i/\eta_o \ll 1$ being the ratio of internal and external shear viscosities), Schnitzer *et al.* (2014) derived an electrophoretic mobility (under a weak electric field E) that is proportional to ζ^{*3}, with ζ^* being the ζ-potential scaled with k_BT/e. This departs radically from the foregoing linear electrokinetic models, even in the Debye–Hückel regime. The theory is for large (but still spherical) bubbles, for which shear stresses exerted by the gas on the gas–liquid interface are neglected due to $\eta_i/\eta_o \ll 1$. This is motivated, in part, by the large κa limit of Booth's theory predicting a vanishing mobility $\sim \zeta^*\eta_i/\eta_o$ as $\eta_i/\eta_o \to 0$. The theory of Schnitzer *et al.* (2014) also goes beyond the weak-field linearization, seeking to address experimental evidence of electrophoretic bubble velocities scaling as E^2 (Kelsall *et al.* 1996). Schnitzer *et al.* predict the mobility scaling as $E^{2/3}$ when the reduced electric field strength $Eae/(k_BT)$ is greater than a threshold that they numerically demonstrated to decrease with increasing ζ^* (k_BT/e is the thermal energy divided by the fundamental charge). Thus, caution must be applied with respect to interpreting theories (including the present work) and experiments that draw on the weak-field approximation. Similar caution may be required when other independent dimensionless parameters are placed into asymptotically large or small regimes.

Singular electrophoretic mobilities are predicted from the asymptotic theory of Schnitzer *et al.* (2014) and the direct computations of Wu *et al.* (2021) for highly charged, but perfectly uniform, fluid spheres. Such behaviour was not evident from the model of Baygents & Saville (1991) or the theory of Booth (1951) (low charge). The singular mobility has been suggested to reflect shortcomings of the Poisson–Boltzmann equilibrium (Wu *et al.* 2021; Majhi & Bhattacharyya 2024), but evidence also points to neglect of physically grounded interfacial exchange and/or interfacial-charge mobility mechanisms, as addressed in the present work. Note also that, as pointed out by an anonymous referee, singular velocity (at unrealistically high ζ-potentials) will

be suppressed by finite/nonlinear advection effects that are absent in the linearized electrokinetic models; this evidently reflects an imperfect pitchfork bifurcation in the parameter space for highly charged interfaces.

Complementary to the theory of Booth (1951), but exclusively under the weak-field assumption, is the model of Ohshima, Healy & White (1984) for mercury drops. Assuming a uniform surface-charge density, an analytical formula was derived for low ζ-potentials, depending on κa and the ratio of the internal and external shear viscosities η_i/η_o. A formula was also derived for arbitrary ζ-potentials with $\kappa a \gg 1$, and both were tested by comparison with numerical solutions of the full electrokinetic model. Schnitzer *et al.* (2013) extended the analysis for sufficiently large mercury drops when the weak-field approximation breaks down. Interestingly, this independently furnished the same mobility as the Levich–Frumkin formula, which Ohshima *et al.* (1984) had suggested was in error due to the discrepancy with their model at higher ζ-potentials. It will be demonstrated in the present work that a sufficiently high dielectric permittivity furnishes the same fluid-sphere mobilities as the theory of Ohshima *et al.* (1984), independent of the interfacial-charge mobility and kinetic exchange, now subject to the weak-field approximation.

Consider now the physical basis on which extant models may be grounded on an assumption of uniform surface charge. If one assumes irreversible surface-charge adsorption, then a uniform surface charge might naively be assumed to reflect a high interfacial-charge mobility, so that diffusion annihilates interfacial-charge perturbations driven by electromigration and advection. However, it must be acknowledged that, at least to a first approximation, charge mobility affects diffusion and electromigration equally. Thus, a high interfacial mobility promotes a dominant balance of diffusion and electromigration. However, this demands a non-uniform interfacial charge, violating the initial assumption.

If one instead considers low or vanishing interfacial-charge mobility, then the interfacial flux may become dominated by advection, which must be balanced by either interfacial exchange or local/singular perturbations to the diffusion and electromigration. This suggests a state of uniform charge as reflecting low interfacial mobility and fast interfacial kinetics, i.e. large interfacial Péclet and Damkökler numbers. Indeed, the computations of Baygents & Saville (1991) were undertaken with zero interfacial mobility (vanishing surface diffusivity $D \to 0$) and fast kinetic exchange (kinetic rate coefficients for adsorption and desorption $k_a, k_d \to \infty$). However, as already stated, it is not clear how these conditions may be achieved from a physical perspective, since the kinetic-exchange rates (for adsorption and desorption) are coupled by thermodynamics, thus prescribing the equilibrium surface-charge density and ζ-potential.

To address the foregoing questions, the present study proposes a fluid-sphere electrokinetic model with interfacial-exchange kinetics, interfacial-charge mobility and Marangoni effects (Baygents & Saville 1991), under the weak-field assumption. The computations undertaken are a steady-state application of the dynamic model of Hill (2020). Here, analytical formulas for the steady internal fluid dynamics and electrostatic polarization of the interior non-ionic/dielectric Newtonian fluid are coupled to a numerical solution of the standard electrokinetic model for the unbounded exterior electrolyte (O'Brien & White 1978). The internal and external fluids are coupled via an interfacial phase, also demanding continuous tangential velocity (no interfacial slip), zero radial velocity (due to surface tension maintaining a spherical interface) and a surface population of interfacial charge subject to interfacial exchange, advection, diffusion and electro-migration. An interfacial momentum balance accounts for fluid shear stresses

(on the internal and external sides), an interfacial electrical force (Maxwell stress) and gradients of interfacial tension (Marangoni force).

Because the surface diffusion and electro-migration fluxes depend on a surface diffusivity D, the principal dimensionless parameter reflecting the surface-charge mobility (for a single adsorbing charged species) is an interfacial Péclet number

$$Pe = \frac{u_c a}{D} = \frac{(k_B T/e)^2 \epsilon_o \epsilon_0}{\eta_o D}, \tag{1.1}$$

where $u_c = (k_B T/e)^2 \epsilon_o \epsilon_0/(\eta_o a)$ is a characteristic 'Smoluchowski' electrophoretic velocity, independent of the applied electric-field strength (Russel *et al.* 1989). Here, $k_B T/e \approx 25$ mV is the thermal energy per unit of fundamental electric charge, and ϵ_o and η_o are the relative dielectric permittivity and shear viscosity of the external electrolyte. For water at room temperature and $D = 10^{-9}$ m^2 s^{-1}, which is representative of a small ion, (1.1) furnishes $Pe \approx 0.5$. Larger ions, such as surfactant macromolecules and Pickering nano-particulates, immobilized at a viscous fluid interface could reasonably present much lower surface mobilities ($D \ll 10^{-9}$ m^2 s^{-1}), thus furnishing $Pe \gg 1$.

Electrophoretic velocities are often linear in the strength of the applied electric field, i.e. $u_c \sim \mu E$, where μ is the electrophoretic mobility and E is the electric-field strength. Under these conditions, another Péclet number, based on the actual electrophoretic velocity, is

$$\mathcal{P}_e = \frac{\mu E a}{D} = \mu^* \frac{\eta_m}{\eta_o} 4\pi \epsilon_o \epsilon_0 a_m a E/e, \tag{1.2}$$

where μ^* is a dimensionless/scaled electrophoretic mobility (defined in the results section). The right-hand side of (1.2) expresses the diffusivity of the molecular tracer in terms of the Stokes–Einstein diffusivity $D = k_B T/(6\pi \eta_m a_m)$ (molecule radius a_m in an environment with shear viscosity η_m). Thus, with a drop/bubble radius $a = 100$ nm, tracer radius $a_m = 0.1$ nm, $\eta_m/\eta_o \sim 1$ and an aqueous electrolyte at room temperature, $\mathcal{P}_e \lesssim 1$ may be achieved by limiting the electric-field strength to $E \lesssim (10^6/\mu^*)$ V m^{-1}, even if $Pe \gtrsim 1$.

The foregoing Péclet number neglects buoyant advection, which may – especially for bubble electrophoresis (Takahashi 2005) – impart a significant translational velocity $u_g = 2\Delta\rho g a^2/(F^* 9\eta_o)$ (density difference $\Delta\rho$, gravitational acceleration g) for which there is another Péclet number

$$\mathcal{P}_g = \frac{u_g a}{D} = \frac{1}{F^*} \frac{2\Delta\rho g a^3}{9\eta_o D}, \tag{1.3}$$

where $F^* \sim 1$ is the drag coefficient. The present work implicitly assumes $u_g \lesssim \mu E$, which is achieved for colloidal drops and bubbles with radius $a \lesssim \sqrt{\mu E \eta/(g\Delta\rho)} \sim 1$ μm.

The present electrokinetic model for the external electrolyte is a standard one by which perturbations in the ion concentrations, electrostatic potential and fluid velocity are truncated to linear order in the applied electric field (O'Brien & White 1978). These equations have been derived and applied in enumerable papers (predominantly on rigid-particle electrophoresis) and, therefore, will not be repeated herein. The computational solution is as detailed by Hill, Saville & Russel (2003) for steady electrophoresis of soft, rigid spheres, modified for interfacial effects as detailed by Hill (2020) in the context of dynamic fluid-sphere electrophoresis. The calculations also furnish the steady drag coefficient F^*, which provides physical insight to help interpret the electrophoretic mobility. The conductivity increment is available, but is reported only to benchmark computations against those of Ohshima *et al.* (1984) for mercury drops.

The interfacial transport model has not previously been applied in the context of steady fluid-sphere electrophoresis, and so it is set out in the theory of § 2. Readers who are not concerned with these details may proceed directly to the results in § 3. Section 3.1 considers fluid spheres with adsorbed charge that is irreversibly bound to the interface with a low ζ-potential. Thus, with zero interfacial exchange and without Marangoni effects, this sub-section focusses on interfacial-charge mobility in a context where comparisons can be made with existing theories (valid in the Debye–Hückel regime). Section 3.2 turns to fluid spheres bearing finite interfacial charge. This expedites direct comparisons with Baygents & Saville (1991), exploring the consequences of a finite kinetic-exchange rate and finite interfacial-charge mobility. Section 3.3 draws comparisons with bubble and drop mobilities computed by Wu *et al.* (2021) based on the standard electrokinetic model with uniform surface charge, and the asymptotic theory of Schnitzer *et al.* (2014) for spherical bubbles with uniform surface charge. This identifies interfacial-charge mobility and kinetic exchange as regularizing the singular mobilities that have been predicted by the standard electrokinetic model for fluid spheres with a high, uniform surface charge. Section 3.4 examines select flows, electrostatic potential and ion-concentration perturbations. Finally, § 3.5 turns to mercury drops (non-ion-conducting, highly polarizable fluid spheres), exploring how interfacial-charge mobility impacts the conclusions drawn from the long-standing model of Ohshima *et al.* (1984). The paper concludes with a brief summary in § 4.

2. Interfacial electrokinetic model

For the external electrolyte, the electrostatic potential ψ, ion concentrations n_i (in the electrolyte), fluid velocity $\boldsymbol{u}$ and pressure p are subject to the standard electrokinetic model (O'Brien & White 1978), linearized for an applied electric-field strength E that is weak compared with the smaller of $\kappa k_B T/e$ or $k_B T/(ae)$. As already highlighted in the introduction, these equations and their numerical solution are well known. The fluid sphere is an uncharged, non-ion-conducting, dielectric Newtonian fluid (relative dielectric permittivity ϵ_i and shear viscosity η_i). The ion concentrations inside the sphere are zero, with electrostatic potential and fluid dynamics that satisfy Laplace's equation and the steady Stokes equations, respectively. Thus, the internal and external fluids are coupled by the interface, which is assumed spherical (radius a), hosting an interfacial population of adsorbed ions. The model for the interface is adapted from that of Hill (2020) for dynamic electrophoresis (in the megahertz frequency range). Whereas Baygents & Saville (1991) assumed that the adsorption–desorption kinetics are rapid compared with ion transport by advection, diffusion and electromigration, the present work adopts a kinetic model for the local exchange of an adsorbing ion between the fluid-sphere interface and the immediately adjacent electrolyte.

2.1. *Conservation equations*

The interfacial/surface concentration (per unit area) of an adsorbing ion is the sum of a uniform equilibrium value c^0 and a perturbation c'

$$c(\boldsymbol{x}) = c^0 + c'(\boldsymbol{x}), \tag{2.1}$$

where $\boldsymbol{x} = a\boldsymbol{e}_r$ identifies position on the spherical interface, relative to the sphere centre (radial unit vector $\boldsymbol{e}_r$, tangential unit vector $\boldsymbol{e}_\theta$). For notational simplicity, a subscript $i = 1, \ldots, N$ to distinguish ion species is discarded due to just one ($i = 1$) of these species adsorbing in the present work.

The surface-ion-conservation equation is

$$0 = -\boldsymbol{\nabla}_s \cdot \left(-D\boldsymbol{\nabla}_s c' - zec^0 \frac{D}{k_B T} \boldsymbol{\nabla}_s \psi' + \boldsymbol{u}_\theta c^0 \right) + k_a n'(r=a) - k_d c', \tag{2.2}$$

where $\boldsymbol{\nabla}_s$ is the surface-gradient operator and $\boldsymbol{u}_\theta$ is the interfacial (tangential) velocity (in the sphere reference frame). The tangential flux comprises lateral diffusion (interface/surface diffusivity D), electro-migration (charge ze) and advection. Note that this flux is linearized with respect to perturbations (primed quantities) from the equilibrium state (superscripts '0'). The interfacial 'source' terms incorporate (first-order) adsorption and desorption coefficients (k_a and k_d) to model exchange between the interface and the immediately adjacent (external) electrolyte.

The ion concentration in the external electrolyte at $\boldsymbol{x} = r\boldsymbol{e}_r$ is

$$n(\boldsymbol{x}) = n^0(r) + n'(\boldsymbol{x}), \tag{2.3}$$

where the equilibrium ion concentration is

$$n^0(r) = n^\infty \exp(-\psi^0(r) ze/(k_B T)). \tag{2.4}$$

Here, n^∞ is the bulk ion concentration (as $r \to \infty$), and $\psi^0(r)$ is the equilibrium electrostatic potential furnished by a numerical solution of the nonlinear Poisson–Boltzmann equation (with prescribed equilibrium surface potential $\zeta = \psi^0(r=a)$ or equilibrium surface-charge density σ^0).

At equilibrium, the adsorption and desorption rates in (2.2) are equal, and so the ratio of the kinetic-exchange coefficients may be related to a prescription of the equilibrium interfacial-charge density. Since the equilibrium concentration of the adsorbing ion at the interface is $n^\infty \exp(-\zeta ze/(k_B T))$, it follows that

$$\frac{k_a}{k_d} = \frac{c^0}{n^\infty \exp(-\zeta ze/(k_B T))}, \tag{2.5}$$

where $\sigma^0 = zec^0$. Note that the ratio has the dimension of length, since k_a has dimensions m s^{-1} (adsorption velocity), and k_d has dimension s^{-1} (frequency).

In addition to the foregoing adsorbed-species conservation equation, there is an interfacial tangential momentum conservation equation (zero interfacial inertia)

$$\boldsymbol{t}_\theta(r=a_-) + \boldsymbol{t}_\theta(r=a_+) - \gamma^0 \beta \boldsymbol{\nabla}_s c' - \sigma^0 \boldsymbol{\nabla}_s \psi' = 0, \tag{2.6}$$

where $\boldsymbol{t}_\theta(r=a_-)$ and $\boldsymbol{t}_\theta(r=a_+)$ are the (tangential) viscous tractions acting on the inside and outside of the interface (outward unit normals $-\boldsymbol{e}_r$ and $\boldsymbol{e}_r$, inside and outside shear viscosities η_i and η_o, respectively), i.e.

$$\boldsymbol{t}_\theta(r=a_-) = -\{-p\boldsymbol{I} + \eta_i[\boldsymbol{\nabla}\boldsymbol{u} + (\boldsymbol{\nabla}\boldsymbol{u})^{\mathrm{T}}]\} \cdot \boldsymbol{e}_r \cdot \boldsymbol{e}_\theta \boldsymbol{e}_\theta \big|_{r=a_-}, \tag{2.7}$$

and

$$\boldsymbol{t}_\theta(r=a_+) = \{-p\boldsymbol{I} + \eta_o[\boldsymbol{\nabla}\boldsymbol{u} + (\boldsymbol{\nabla}\boldsymbol{u})^{\mathrm{T}}]\} \cdot \boldsymbol{e}_r \cdot \boldsymbol{e}_\theta \boldsymbol{e}_\theta \big|_{r=a_+}. \tag{2.8}$$

Moreover, $-\gamma^0 \beta \boldsymbol{\nabla}_s c'$ is the resultant interfacial tension/Marangoni traction ($\gamma^0 \beta \equiv \partial \gamma^0 / \partial c^0 |_{c^0}$ with γ^0 the equilibrium interfacial tension), and $-\sigma^0 \boldsymbol{\nabla}_s \psi'$ the resultant (tangential) electrical/Maxwell traction.

Finally, Gauss's law at the interface ($\boldsymbol{x} = a\boldsymbol{e}_r$) is

$$\epsilon_i\epsilon_0\nabla\psi' \cdot \boldsymbol{e}_r|_{r=a_-} - \epsilon_o\epsilon_0\nabla\psi' \cdot \boldsymbol{e}_r|_{r=a_+} = \sigma'(\boldsymbol{x}), \tag{2.9}$$

where the interfacial/surface-charge density is

$$\sigma(\boldsymbol{x}) = \sigma^0 + \sigma'(\boldsymbol{x}) = \sigma^0 + zec'(\boldsymbol{x}). \tag{2.10}$$

Since there is no space charge inside the sphere, the equilibrium interfacial/surface-charge density is

$$\sigma^0 = -\epsilon_o\epsilon_0 \left.\frac{\partial\psi^0}{\partial r}\right|_{r=a_+}. \tag{2.11}$$

For the single adsorbing species, $\sigma^0 = zec^0$, e.g. as furnished by an equilibrium adsorption isotherm or prescribed equilibrium surface potential $\zeta = \psi^0(r = a)$.

2.2. *Linearized solution*

From the solution of Stokes equations inside the sphere, the tangential velocity and hydrodynamic traction at the interface (unit normal $-\boldsymbol{e}_r$) can be written

$$\boldsymbol{u}_\theta(r = a_-) = C_1 a c_u \boldsymbol{X} \cdot \boldsymbol{e}_\theta \boldsymbol{e}_\theta, \tag{2.12}$$

and

$$\boldsymbol{t}_\theta(r = a_-) = -\eta_i C_1 c_t \boldsymbol{X} \cdot \boldsymbol{e}_\theta \boldsymbol{e}_\theta, \tag{2.13}$$

where C_1 is an integration constant that prescribes the interface velocity and viscous shear stress. When the Stokes equations are scaled using κ^{-1} as the characteristic length, $c_u = -2/(\kappa a)$ and $c_t = -6/(\kappa a)$. Note that $\boldsymbol{X}$ is either a uniform translation of the electrolyte $\boldsymbol{U}$ (velocity relative to a stationary sphere) in the absence of an electric field or an electric field $\boldsymbol{E}$ applied to a stationary sphere (O'Brien & White 1978).

The electrostatic potential satisfying Laplace's equation inside the sphere ($r < a$) is

$$\psi(\boldsymbol{x}) = \psi^0 + \psi'(\boldsymbol{x}) = \psi^0 + [\hat{\psi}(r = a)(r/a) - r(E/X)]\boldsymbol{X} \cdot \boldsymbol{e}_r, \tag{2.14}$$

where ψ^0 and $\hat{\psi}(r = a)$ are constants. Note that the electrostatic potential is continuous across the interface, a consequence of implicitly prescribing zero interfacial dipole moment (Baygents & Saville 1991).

Outside the sphere, there are differential conservation equations for N ionic species, and fluid mass and momentum. With Gauss's law, these furnish the standard electrokinetic model (O'Brien & White 1978). The equations are solved (for $r > a$) in terms of the following independent variables (ion concentrations, electrostatic potential and fluid velocity):

$$n_i(\boldsymbol{x}) = n_i^0(r) + \hat{n}_i(r)\boldsymbol{X} \cdot \boldsymbol{e}_r, \quad i = 1, \ldots, N, \tag{2.15}$$

$$\psi(\boldsymbol{x}) = \psi^0(r) - r\boldsymbol{E} \cdot \boldsymbol{e}_r + \hat{\psi}(r)\boldsymbol{X} \cdot \boldsymbol{e}_r, \tag{2.16}$$

and (Hill *et al.* 2003)

$$\boldsymbol{u}(\boldsymbol{x}) = \boldsymbol{U} + \nabla \times \nabla \times [h(r)\boldsymbol{X}]. \tag{2.17}$$

Superscripts '0' identify (spherically symmetric) equilibrium, and hatted variables identify spherically symmetric (radial) contributions to the total perturbation. One may also

express the velocity as (Hill & Afuwape 2020)

$$\boldsymbol{u}(\boldsymbol{x}) = \boldsymbol{\nabla} \times [f(r)\boldsymbol{X} \times \boldsymbol{e}_r] = (f_r + fr^{-1})\boldsymbol{X} + (-f_r + fr^{-1})\boldsymbol{X} \cdot \boldsymbol{e}_r \boldsymbol{e}_r, \tag{2.18}$$

giving

$$f = rU/(2X) - h_r, \quad f_r = U/(2X) - h_{rr}, \quad \text{and} \quad f_{rr} = -h_{r,rr} = -g, \tag{2.19a–c}$$

where $g \equiv h_{r,rr}$ is an auxiliary variable to avoid derivatives in the numerical solution for $h(r)$ that are higher than of second order.

To couple the N ion-conservation equations in the standard electrokinetic model to the interface, the (Nernst–Planck) ion fluxes at the interface are required to satisfy

$$\left(-D_i \boldsymbol{\nabla} n_i' - \boldsymbol{\nabla}\psi' z_i e n_i^0 \frac{D_i}{k_B T} + n_i^0 \boldsymbol{u}\right) \cdot \boldsymbol{e}_r \bigg|_{r=a} = k_d c_i' - k_a n_i'(r=a), \quad i = 1 \tag{2.20}$$

$$\left(-D_i \boldsymbol{\nabla} n_i' - \boldsymbol{\nabla}\psi' z_i e n_i^0 \frac{D_i}{k_B T} + n_i^0 \boldsymbol{u}\right) \cdot \boldsymbol{e}_r \bigg|_{r=a} = 0, \quad i = 2, \ldots, N, \tag{2.21}$$

where $i = 1$ identifies the (single) adsorbing species (subscripts discarded above).

The foregoing may be generalized to multiple adsorbing species, albeit by introducing additional kinetic-exchange coefficients. Note that D_i are the ion diffusivities (in the external electrolyte), which are generally prescribed as $D_i = k_B T/\gamma_i$ with γ_i the friction coefficient calculated from the limiting molar conductivity (λ_i).

At the interface ($\boldsymbol{x} = a\boldsymbol{e}_r$), linearity and symmetry require an interfacial concentration perturbation of the form

$$c'(\boldsymbol{x}) = d_c \boldsymbol{X} \cdot \boldsymbol{e}_r, \tag{2.22}$$

where d_c is a constant that measures the interfacial concentration polarization.

2.3. *Computational implementation*

Substituting (2.22) and the other independent variables into the foregoing conservation equations and boundary conditions furnishes the following $N + 5$ independent (algebraic and differential) relationships (boundary conditions) at $r = a$.

(i) Zero radial velocity

$$h_r = aU/(2X). \tag{2.23}$$

(ii) Interfacial (tangential) momentum conservation

$$-(\eta_i/\eta_o)C_1 c_t - g = [\gamma^0 \beta d_c + \sigma^0(\hat{\psi} - aE/X)]/(a\eta_o). \tag{2.24}$$

(iii) Continuous tangential velocity

$$h_{rr} = U/(2X) - C_1 a c_u. \tag{2.25}$$

(iv) Interfacial Gauss condition

$$\epsilon_i\epsilon_0(\hat{\psi}/a - E/X) - \epsilon_o\epsilon_0(\hat{\psi}_r - E/X) = z d_c e. \tag{2.26}$$

(v) Interfacial species conservation (for the adsorbing ion species, $i = 1$)

$$-(D + k_d a^2/2)d_c + k_a \hat{n}_1 a^2/2 - (\hat{\psi} - aE/X) z e c^0 \frac{D}{k_B T} = -c^0 C_1 a^2 c_u. \tag{2.27}$$

(vi) N radial ion fluxes

$$-k_d d_c + k_a \hat{n}_i = D_i \hat{n}_{i,r} + \psi_r^0 z_i e \hat{n}_i \frac{D_i}{k_B T} + (\hat{\psi}_r - E/X) z_i e n_i^0 \frac{D_i}{k_B T}, \quad i = 1 \tag{2.28}$$

$$0 = D_i \hat{n}_{i,r} + \psi_r^0 z_i e \hat{n}_i \frac{D_i}{k_B T} + (\hat{\psi}_r - E/X) z_i e n_i^0 \frac{D_i}{k_B T}, \quad i = 2, \ldots, N. \tag{2.29}$$

These are coupled to $N + 3$ independent differential relationships (ordinary differential equations) for the external electrolyte ($r > a$). More generally, with M adsorbing ions ($1 \leqslant M \leqslant N$), the interfacial model contributes a net $M + 1$ independent relationships to uniquely determine $M + 1$ unknowns (e.g. C_1 and d_c for $M = 1$).

2.4. *Parametric considerations*

When the interfacial model is expressed in a dimensionless form that is compatible with the scaled electrokinetic conservation equations for the electrolyte ($r > a$), several additional independent dimensionless parameters are revealed. In addition to κa, $\zeta e/(k_B T)$, ϵ_i/ϵ_o and $Pe_i = u_c/(\kappa D_i)$ (Hill *et al.* 2003), there are $Pe = u_c a/D$ (defined in the introduction), η_i/η_o, $k_d a^2/D$, $k_a a/D$ and

$$Ma = \frac{\gamma^0 \beta}{k_B T} = Ma_c \frac{\eta_o D}{k_B T c^0 a}. \tag{2.30}$$

These characterize the internal fluid dynamics, interfacial Marangoni effects (due to surface tension and interfacial transport) and exchange kinetics. The concentration Marangoni number

$$Ma_c = \frac{\gamma^0 \beta c^0 a}{\eta_o D}, \tag{2.31}$$

compares interfacial diffusion and surface-tension relaxation times, whereas Ma is a dimensionless combination of intrinsic interfacial properties (comparing interfacial and thermal energy) (Hill & Afuwape 2020).

Note that, since k_a and k_d are constrained by the equilibrium condition (2.5), adopting k_d as the independent kinetic-exchange rate, its dimensionless counterpart is a Damköhler number

$$Da = \frac{k_a a}{D} = \frac{k_d a}{D} \frac{c^0}{n^\infty \mathrm{e}^{-\zeta^* z}}, \tag{2.32}$$

which compares the kinetic-exchange rate k_a with a diffusion velocity. Another convenient Damköhler number (comparing k_d with a diffusion frequency D/a^2) is $k_d a^2/D$. Of course, other (dependent) dimensionless groups may be formed, e.g. drawing on Pe to assess the role of interfacial advection, etc.

In this work, a combination of dimensionless and dimensional variables is adopted in presenting the results. This is motivated, in part, by familiarity with customary dimensionless variables, such as κa and ζ^*, and the less familiar dimensional k_d and D, which separately target interfacial exchange and interfacial mobility, but appear combined in (2.32). For this, it is necessary to consider whether or not n^∞ in (2.32) varies with the

Debye length and ionic strength

$$\kappa^{-1} = \sqrt{\frac{\epsilon_o \epsilon_0 k_B T}{2 I e^2}}, \quad I = \frac{1}{2}\sum_{i=1}^{N} z_i^2 n_i^\infty. \tag{2.33a,b}$$

Thus, if the adsorbing ion has a trace concentration (e.g. an ionic surfactant) among those in a supporting electrolyte (comprising only non-adsorbing species), then n^∞ may be considered independent of κ^{-1}, in which case Da will vary only according to the coupling of ζ and σ^0 by κa. On the other hand, if the adsorbing ion is part of the electrolyte that dominates the bulk ionic strength I, then Da may also vary (perhaps significantly) with $n^\infty \sim I \sim \kappa^2$ when k_d is a prescribed constant. The highly coupled physics and resulting distribution of k_d and D (and others) among multiple dimensionless groups motivates a more physically motivated, hybrid approach for exploring the broader parameter space.

3. Results

The electrophoretic mobility $\mu = -U/E$ is the ratio of the electrophoretic velocity $-U$ to the strength of the applied electric field E. The results below are presented in terms of a scaled electrophoretic mobility defined as

$$\mu^* = \mu \frac{3\eta_o}{2\epsilon_o \epsilon_0 k_B T/e}. \tag{3.1}$$

For weakly charged spheres, the mobility is linear in the scaled surface potential

$$\zeta^* = \zeta \frac{e}{k_B T}, \tag{3.2}$$

thus motivating plots of μ^*/ζ^*. As convenient points of reference, the well-known Hückel and Smoluchowski values for rigid spheres when $|\zeta| \lesssim k_B T/e \approx 25$ mV are $\mu^* = 1$ and $3/2$ for $\kappa a \ll 1$ and $\kappa a \gg 1$, respectively.

A drag coefficient is defined as

$$F^* = \frac{F_d}{6\pi\eta_o a U}, \tag{3.3}$$

which is the ratio of the drag force F_d under translation at velocity $-U$ to the Stokes drag force, $6\pi\eta_o a U$. For uncharged rigid spheres (without electro-viscous effects), $F^* = 1$, and, for uncharged inviscid spheres ($\eta_i/\eta_o \to 0$), the well-known Hadamard–Rybczynski theory

$$F^* = \frac{2/3 + \eta_i/\eta_o}{1 + \eta_i/\eta_o} \tag{3.4}$$

furnishes $F^* = 2/3$.

3.1. *Debye–Hückel regime, irreversibly bound charge*

This subsection focusses on weakly charged interfaces for which analytical formulas are available to provide benchmark points of reference. The computations are undertaken with an aqueous electrolyte containing two pairs of ions: Na^+ and DS^- (dodecyl sulphate) having (trace) bulk concentration 10^{-10} mol l^{-1}; and Na^+ and Cl^- (added salt) having a bulk concentration that is adjusted to achieve a prescribed value of κa. Here, DS^- is the

(irreversibly) adsorbing ion for which $k_d = 0$. Note that the calculations do not seek to model the surfactant adsorption, since this would demand the surface-charge density (and ζ-potential) to be a specific function (isotherm) of the bulk electrolyte composition.

In the Debye–Hückel regime for which $|\zeta^*| \lesssim 1$ and μ^* is proportional to ζ^*, the ratio μ^*/ζ^* is plotted vs κa for viscosity ratios η_i/η_0 in the range 10^{-3}–10^3. Note that, with fixed $|\zeta^*| \lesssim 1$, the interfacial-charge density varies with κa according to

$$\zeta = \frac{\sigma^0 a}{\epsilon_o \epsilon_0 (1 + \kappa a)}. \tag{3.5}$$

Thus, an increase in κa when $\kappa a \gg 1$ is implicitly accompanied by a commensurate increase in σ^0.

In figure 1, the surface potential is extremely small ($\zeta^* = -0.001$, corresponding to $\zeta \approx -0.025$ mV) with an extremely high (unphysical) interfacial mobility ($D = 10^{-6}$ m^2 s^{-1} furnishing $Pe \approx 5.15 \times 10^{-4}$). In panel ($a$) with $\epsilon_i/\epsilon_o \ll 1$, the computations agree with the theory of Booth (1951), but only when $\kappa a \lesssim 100$. For rigid spheres (achieved with $\eta_i/\eta_0 \gg 1$), the computations furnish the well-known Henry mobility (Russel *et al.* 1989). In panel (b) with $\epsilon_i/\epsilon_o = 1$, Booth's theory, evaluated here with (internal conductivity parameter) $\lambda \approx 0$ (equi-conducting sphere), furnishes the Hückel mobility, independent of the viscosity. Note that the computations are in good agreement with the theory of Mahapatra *et al.* (2022) when $\kappa a \lesssim 100$; departures from the analytical theories in panels (a,b) when $\kappa a \gg 1$ are attributed to the interfacial-charge mobility, as explored below by varying Pe and ζ^*.

The very large value of ϵ_i/ϵ_o for the results in figure 1(c) is difficult to justify from a practical perspective, since there are few, if any, non-ion-conducting fluids with a higher dielectric permittivity than of water. Nevertheless, these results test the computational fidelity and provide physical insight, e.g. addressing how large ϵ_i/ϵ_o must be for the mobility to approximate that of a metallic fluid, such as mercury. Here, the computations cannot be distinguished from the theory of Mahapatra *et al.* (2022) at any value of κa, thus validating, in part, the computational accuracy. The small quantitative departure of the theory of Ohshima *et al.* (1984) (dotted lines) from the computations when $\kappa a \gtrsim 100$ in panel (c) reflects the large but finite value of $\epsilon_i/\epsilon_o = 10^3$, whereas the mobilities according to Ohshima *et al.* (1984) for mercury drops emerge as $\epsilon_i/\epsilon_o \to \infty$.

Note that the accompanying drag coefficients (not shown) are computed equal to their respective Hadamard–Rybczynski values; this indicates fluid-behaving interfaces without electro-viscous effects, as is to be expected at low interfacial-charge densities. The velocity scale for mercury drops (and therefore the electrophoretic mobility) is $O(\kappa a)$ larger than the Smoluchowski scale $u_S = (k_B T/e)^2 \epsilon_o \epsilon_i/(\eta_o a)$ (Schnitzer *et al.* 2013). This is evident upon recognizing the interfacial charge per unit area from (3.5) as $\sim \zeta \kappa \epsilon_o \epsilon_0$, the interfacial electric field (on the diffuse part of the double layer) as $\sim E$, thus furnishing an interfacial Maxwell stress $\sim \zeta \kappa \epsilon_o \epsilon_0 E$. Balancing this with $\sim (\eta_o + \eta_i) u_c/a$ the viscous stress from each side of the interface furnishes a large characteristic mobility $u_c/E \sim \kappa a \zeta \epsilon_o \epsilon_0/(\eta_o + \eta_i)$. In this thin double-layer limit, the theory of Schnitzer *et al.* (2013) furnishes corrections to the weak-field approximation, which emerge at moderate ζ-potentials, as highlighted in § 3.5.

Note that computations (not shown) with $\zeta^* = -0.001$ (as in figure 1), but with a much lower interfacial-charge mobility ($Pe \approx 515$) furnished electrophoretic mobilities that are practically the same as in figure 1 ($Pe \ll 1$). The drag coefficients, however, deviate moderately from their Hadamard–Rybczynski values when $\kappa a \gg 1$, even with $\zeta^* = -0.001$. Since the interfacial charge is irreversibly bound to the interface here ($k_d = 0$),

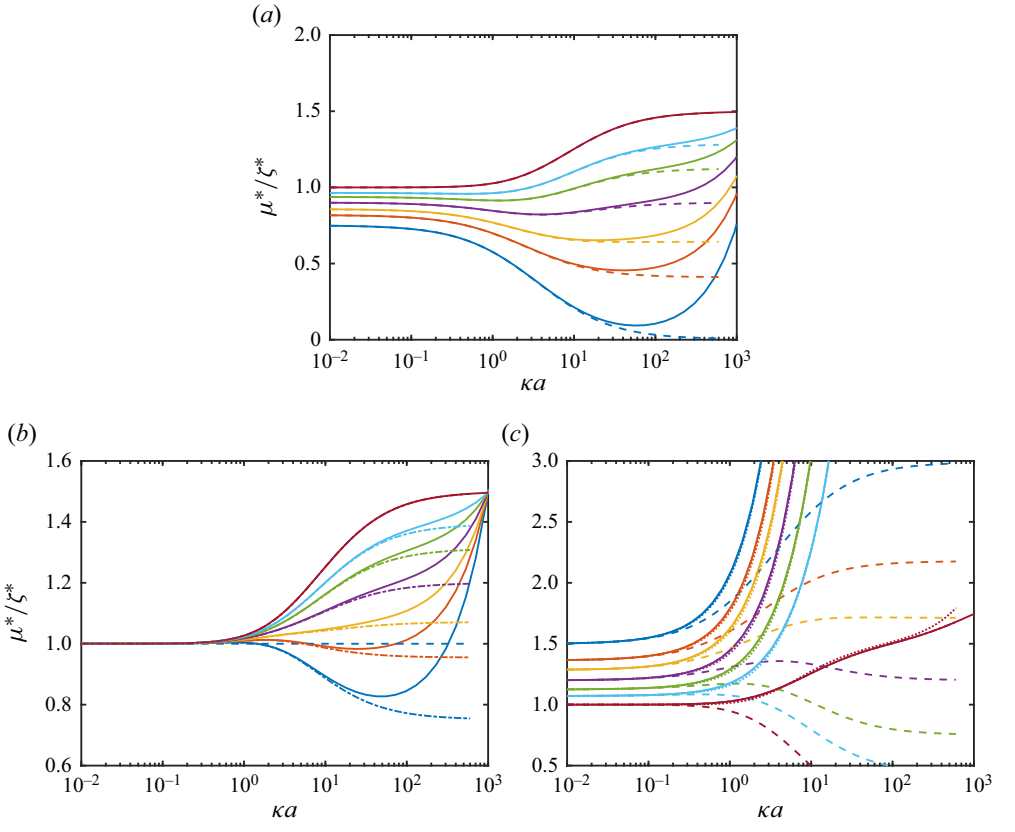

Figure 1. Scaled electrophoretic mobility μ^* vs κa for extremely weakly charged drops and bubbles: $\zeta^* = -0.001$; $\eta_i/\eta_o = 0.001$ (blue), 0.25, 0.5, 1, 2, 4, 10^3 (ruby); $\epsilon_i/\epsilon_o = 10^{-3}$ (*a*), 1 (*b*), 10^3 (*c*). Solid lines are computations (with no surface exchange or Marangoni stresses, high surface diffusivity furnishing $Pe \ll 1$). Dashed lines are the theory of Booth (1951) with $\lambda \approx 0.5$ (*a*, non-conducting/polarizable), 0 (*b*, equi-conducting/polarizable, independent of η_i/η_o) and -1 (*c*, highly conducting/polarizable); dashed-dotted lines in (*b*) are the theory of Mahapatra *et al.* (2022), which equals Booth's theory in (*a*) and overlaps the full computations in (*c*); and dotted lines in (*c*) are the theory of Ohshima *et al.* (1984), which is equivalent to the theory of Mahapatra *et al.* when $\epsilon_i/\epsilon_o \to \infty$. Computed drag coefficients (not shown) are the respective Hadamard–Rybczynski values for all κa.

a vanishing interfacial mobility demands a stationary interface, since otherwise there would be a non-zero interfacial divergence of the surface flux. In this limit, hydrodynamic friction exerted on a stationary interfacial ion population arrests the interface; this state may also be considered as arising from the tangential electrical (Maxwell) traction being balanced by hydrodynamic shear, which must be attributed to the external electrolyte when $\eta_i/\eta_o \ll 1$.

In figure 2, the surface potential has been increased to furnish $|\zeta^*| = 0.1$. Despite being well within the Debye–Hückel regime, the mobilities for $\epsilon_i/\epsilon_o = 10^{-3}$ and 1 in panels (*a*,*b*) are completely different than their counterparts in figure 1. These now exhibit striking departures from the theory of Booth (1951) in panel (*a*) and from the theory of Mahapatra *et al.* (2022) in panel (*b*). Note that the computed mobilities exclusively increase with κa and decrease with increasing η_i/η_o, as for highly polarizable but non-ion-conducting spheres. With $\epsilon_i/\epsilon_o = 10^3$ in panel (*c*), the mobilities depart only slightly from the theories of Ohshima *et al.* (1984) ($\epsilon_i/\epsilon_o = \infty$, dotted lines) and Mahapatra *et al.* (2022) (evaluated

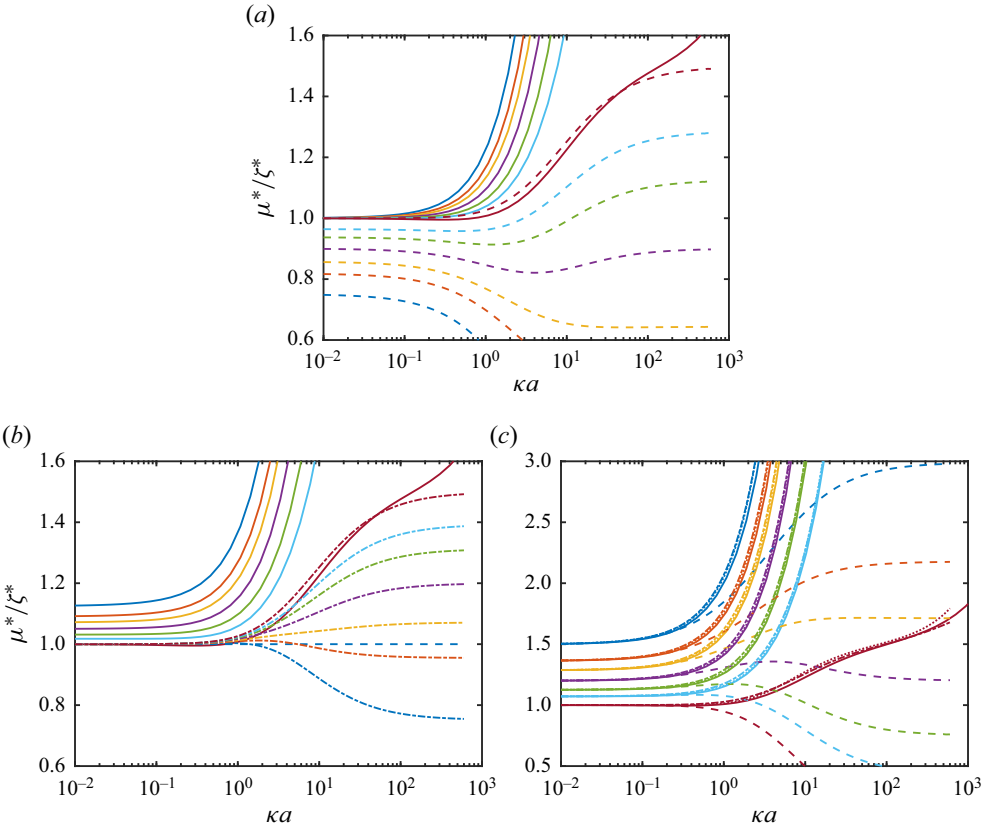

Figure 2. The same as figure 1 ($Pe \ll 1$), but with $\zeta^* = -0.1$: $\epsilon_i/\epsilon_o = 10^{-3}$ (*a*), 1 (*b*), 10^3 (*c*). These mobilities (solid lines) exemplify fluid spheres behaving as highly polarizable fluid spheres on account of high interfacial-charge mobility. Computed drag coefficients (not shown) depart weakly from their respective Hadamard–Rybczynski values.

here with $\epsilon_i/\epsilon_o = \infty$, dashed-dotted lines). Note that the accompanying drag coefficients (not shown) exceed their respective Hadamard–Rybczynski values when $\kappa a \gtrsim 1$.

Computations (not shown) with $\zeta^* = -1$ and $Pe \ll 1$ furnished the same scaled mobilities as in figure 2 with $\zeta^* = -0.1$ and $Pe \ll 1$. Thus, figure 2 unveils high interfacial-charge mobility as suppressing the interfacial tangential electric field, so that the electrical force on the diffuse part of the double layer is balanced by hydrodynamic shear. Since the charge in the double layer increases in proportion to κa when $\kappa a \gg 1$, the shear rates must increase in proportion to κa, manifesting in a proportional increase in the mobility.

Figure 3 shows that decreasing the interfacial-charge mobility to furnish $Pe \gg 1$ (with $|\zeta^*| = 1$) transforms fluid spheres with $\epsilon_i/\epsilon_o = 10^{-3}$ and 1 in panels (*a*,*b*) to their almost perfectly rigid counterparts. The accompanying drag coefficients (not shown) suggest rigid interfaces without significant electro-viscous effects, i.e. $F^* \approx 1$ for all κa. Accordingly, the electrophoretic mobilities are well approximated by the Henry theory ($|\zeta^*| \ll 1$, arbitrary κa). With $\epsilon_i/\epsilon_o = 10^3$ in panel (*c*), the drag coefficients demonstrate a much more gradual, but significant, transition from fluid to rigid behaviour when increasing κa. Interestingly, with $\kappa a \ll 1$, the mobilities depart from all the extant theoretical formulas, tending to the theory of Ohshima *et al.* (1984) for small viscous spheres ($\kappa a \lesssim 1$, $\eta_i/\eta_o \gtrsim 1$), otherwise to the Henry theory when $\eta_i/\eta_o \gg 1$.

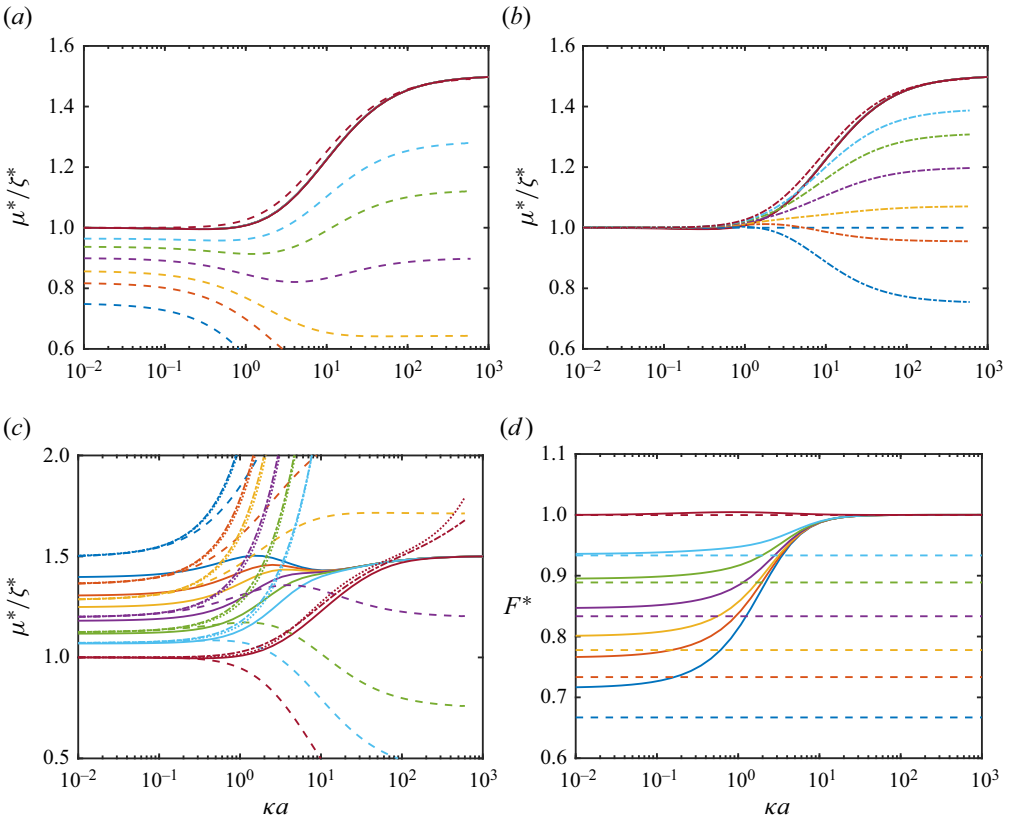

Figure 3. The same as figure 1, but with $\zeta^* = -1$ and $Pe \approx 515$: $\epsilon_i/\epsilon_o = 10^{-3}$ (*a*), 1 (*b*), 10^3 (*c*). These mobilities (solid lines) exemplify fluid spheres behaving as rigid spheres on account of low interfacial-charge mobility. Panel (*d*) shows the drag coefficients and their respective Hadamard–Rybczynski values (dashed lines) accompanying the mobiles in panel (*c*). The drag coefficients accompanying the mobilities in (*a*,*b*) (not shown) are $F^* \approx 1$ (Stokes drag for rigid spheres).

3.2. *Drops with finite ζ-potentials: Baygents & Saville (1991)*

This section revisits figure 1 of Baygents & Saville (1991), which is for non-conducting fluid spheres in an aqueous KCl electrolyte with $\kappa a = 100$ and zero interfacial-charge mobility for which 'ions adsorbed in the interface are equilibrated with those in solution immediately adjacent to the surface'. Accordingly, the results in figure 4 were calculated with adsorption of the K^+ ion (consistent with $\zeta^* > 0$), $D \to 0$ and $k_d \to \infty$.

In the Debye–Hückel regime ($|\zeta^*| \lesssim 1$), (2.32) and (3.5) identify the Damköhler number varying with κa and ζ^* as

$$Da = k_d \frac{k_B T \epsilon_o \epsilon_0}{z D n^\infty e^2} (1 + \kappa a) \mathrm{e}^{\zeta^* z} \zeta^*, \tag{3.6}$$

with $\sigma^0 = zec^0$ and $z\zeta^* > 0$. For an aqueous electrolyte at room temperature with $n^\infty = 1$ mM and $D = 10^{-9}$ m^2 s^{-1}, the dimensional factor $k_{d,0} \equiv Dn^\infty e^2/(k_B T \epsilon \epsilon_0) \sim 10^6$ s^{-1} identifies a characteristic scale for k_d. While the prescription of $D \to 0$ corresponds to $Da \to \infty$, it should be noted that kinetic exchange also couples with diffusion in the external electrolyte, for which another Damköhler number $Da\, D/D_1$ remains finite and, therefore, potentially influential when varying κa and ζ^*.

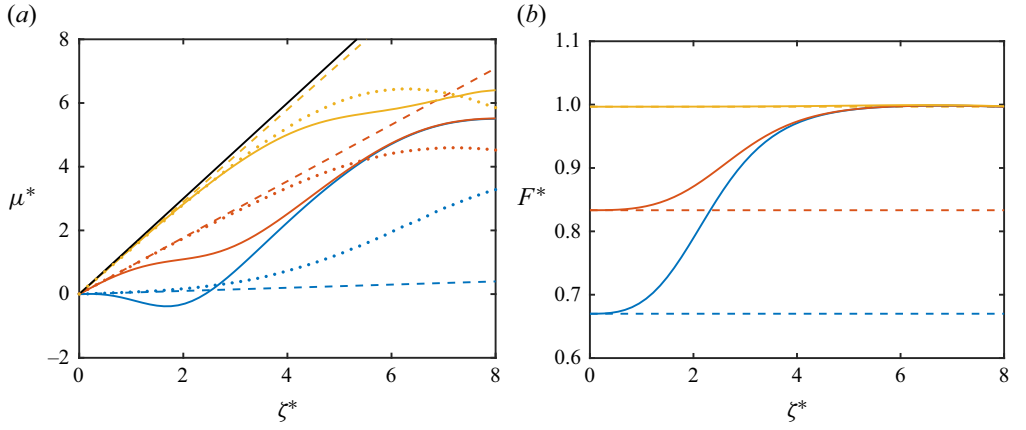

Figure 4. Scaled electrophoretic mobility μ^* (*a*) and drag coefficient F^* (*b*) vs ζ^* for the non-conducting fluid spheres considered in figure 1 of Baygents & Saville (1991) (aqueous KCl electrolyte, shown as dots): $\kappa a = 100$ ($a = 500$ nm), $\eta_i/\eta_o = 0.01$ (blue), 1 (red), 100 (yellow). Other parameters: $\epsilon_i/\epsilon_o = 10^{-3}$, $Pe \gg 1$ ($D = 10^{-15}$ m^2 s^{-1}), $k_d = 10^{12}$ s^{-1}. Dashed lines in (*a*) are the theory of Booth (1951) with $\lambda = 0.5$ (non-conducting drops), and the solid black line in (*a*) is the Smoluchowski mobility (rigid spheres, $\zeta^* \lesssim 1$, $\kappa a \gg 1$). Dashed lines in (*b*) are the Hadamard–Rybczynski drag coefficients.

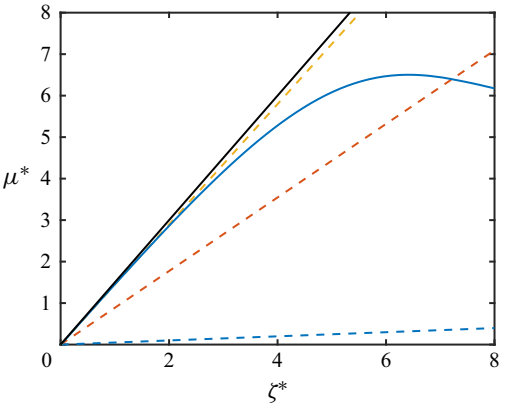

Figure 5. The same as figure 4 ($\kappa a = 100$), but with $k_d = 100$ s^{-1} and $\eta_i/\eta_o = 0.01$. Calculations with $\eta_i/\eta_o = 1$ and 100 (not shown) produce the same mobilities, which are those of rigid spheres in KCl according to O'Brien & White (1978). The drag coefficient is computed $F^* \approx 1$ for all $\zeta^* \gtrsim 0.2$.

Similarly to Baygents & Saville (1991), the mobilities in figure 4 for small enough ζ^* agree with Booth's theory (dashed lines). At higher values of ζ^*, however, there are notable departures of the present model from the computations of Baygents & Saville. For the low-viscosity drops ($\eta_i/\eta_o = 0.01$, blue lines), Baygents & Saville report exclusively positive mobilities (for $\zeta^* > 0$), whereas the mobilities in figure 4 take negative values at intermediate ζ-potentials. For high-viscosity drops ($\eta_i/\eta_o = 100$, yellow lines), Baygents & Saville register mobilities that are very close to those of rigid spheres, as computed by O'Brien & White (1978) (see figure 5 for $\kappa a = 100$).

Note that calculations with other small but finite values of ϵ_i/ϵ_o did not affect the results, neither did other large but finite values of k_d. The mobilities were also invariant to a significant decrease in the sphere radius (e.g. from $a = 500$ to 5 nm), provided that

the values of κa and $k_d a^2/D_1$ were maintained by adjusting κ and k_d accordingly (with $D_1 \approx 1.96 \times 10^{-9}$ m^2 s^{-1} for K$^+$).

Consider now the mobilities of the high-viscosity drops ($\eta_i/\eta_o = 100$) with high ζ-potentials. With zero interfacial-charge mobility, the interfacial current (surface-ion flux) is solely by interfacial advection, which vanishes with sufficiently high drop viscosity. Nevertheless, the interfacial charge may still adjust to local changes in the concentration of the adsorbing ion in the immediately adjacent electrolyte. Moreover, for highly charged interfaces, electromigration polarizes the electrolyte, thus producing an excess and deficit of the adsorbing ion at opposite poles of the drop. Therefore, under conditions that conventionally lead to strong diffuse-layer polarization, e.g. $|\zeta^*| \gtrsim 1$, there is also an interfacial-charge polarization that causes the mobilities in figure 4 ($\eta_i/\eta_o = 100$, yellow lines) when ζ^* is large to depart from those of rigid spheres bearing uniform surface charge (O'Brien & White 1978) (see figure 5 for $\kappa a = 100$).

Note that experimental evidence for a change in the sign of the electrophoretic mobility for small spherical bubbles was reported by Alty (1924). These authors noted a change in the direction of bubble migration occurring for intermediate bubble sizes during a progressive decrease in the bubble size (due to gas absorption). This occurred only for the first bubble introduced into their electrophoresis cell when using highly purified (twice distilled and boiled) water. The observation serves to highlight an extreme sensitivity of bubble mobilities to interfacial phenomena, as explored briefly below by varying κa and k_d. Taken together, the effects of bubble size, interfacial-charge density and kinetic-exchange rate may explain some of the unusual observations of Alty (1924). Note, however, that there is no obvious reason to believe that any of the charge on the bubbles in their experiments had a vanishing interfacial mobility.

Figure 5 shows the mobility for the same drops in figure 4, but with a much smaller kinetic-exchange rate, $k_d = 100$ s^{-1}. Because D is so small, this still furnishes $k_d a^2/D \sim 10^4 \gg 1$, but now the kinetic-exchange rate is small compared with the characteristic interfacial advection rate, thus furnishing a $k_d a^2/(D\,Pe) \sim 0.1$ with $Pe \sim 10^5$ and $k_d a^2/D_1 \sim 0.01$. This makes the adsorption practically irreversible (on the advective time scale), so the vanishing interfacial mobility and kinetic exchange require a vanishing interfacial velocity, since otherwise (in the absence of interfacial electromigration and diffusion) there would be a non-zero divergence of the interfacial current (surface-ion flux). Accordingly, the interfaces are completely arrested, irrespective of the drop viscosity, and the drop mobilities are those of rigid spheres bearing uniform surface charge. It is readily verified that the fluid-sphere mobilities in figure 5 are those of rigid spheres in KCl electrolyte, as furnished by the standard electrokinetic model (O'Brien & White 1978). Note that the same conclusions are drawn from computations with $\kappa a = 1$ under these conditions.

Figure 6 shows the mobility and drag coefficient with $\kappa a = 1$ and 10, all other parameters the same as in figure 4. These highlight the transition from Booth's fluid-sphere mobilities at low ζ-potentials to the rigid-sphere mobilities of O'Brien & White (1978) at high ζ-potentials. The transition is accompanied by increases in the drag coefficient from the Hadamard–Rybczynski values to those of rigid spheres (enhanced by electro-viscous effects at high ζ^*, furnishing $F^* > 1$). Whereas the mobilities for $\kappa a = 10$ depart from those of Baygents & Saville (1991) at intermediate ζ-potentials, the values for $\kappa a = 1$ are practically indistinguishable. This seems to reflect the total polarization being dominated by that of the diffuse layer when $\kappa a = 1$.

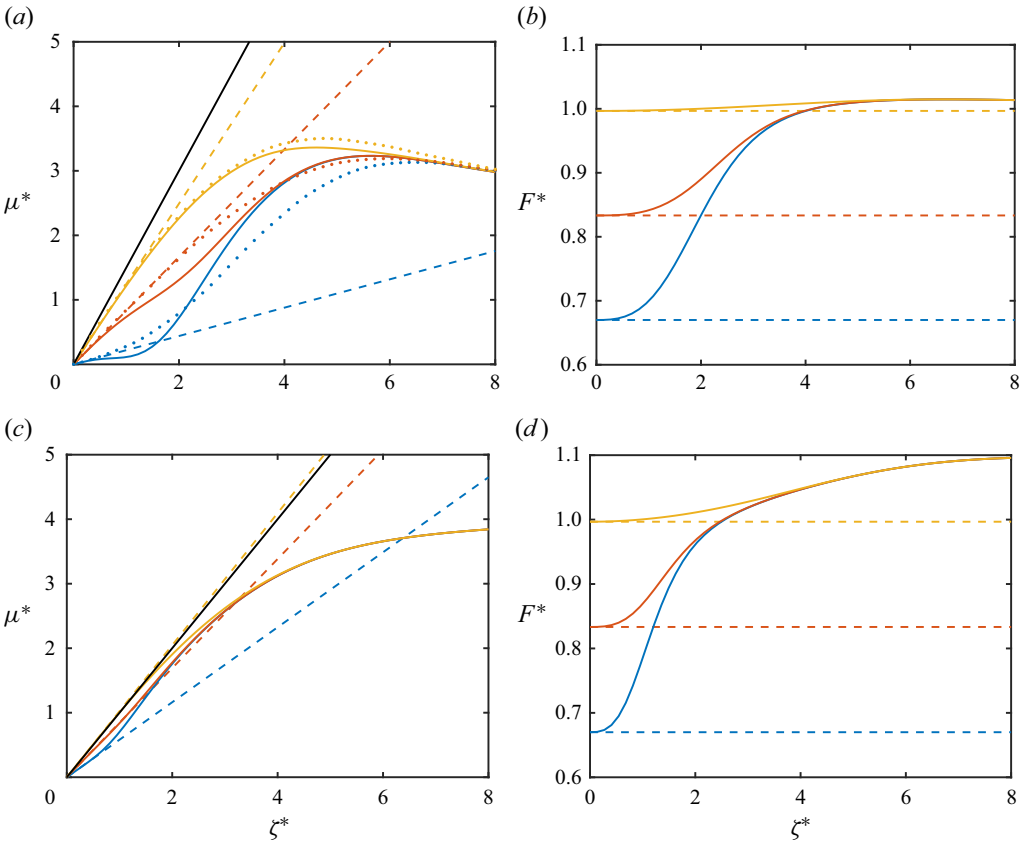

Figure 6. The same as figure 4 ($k_d = 10^{12}$ s^{-1}), but with $\kappa a = 10$ (*a*,*b*) and 1 (*c*,*d*). Dotted lines in (*a*) are from Baygents & Saville (1991) (aqueous KCl electrolyte). Solid black lines in (*a*,*c*) are, respectively, the Smoluchowski and Hückel mobilities (rigid spheres, $\zeta^* \lesssim 1$).

3.3. *Bubbles with finite ζ-potentials: Schnitzer et al. (2014) and Wu et al. (2021)*

Computations were undertaken to compare with the thin double layer of Schnitzer *et al.* (2014) which, recall, predicts a bubble mobility under the weak-field approximation scaling as $\mu^* \sim \zeta^{*3}$ for $|\zeta^*| \lesssim 1$. Here, the electrolyte comprises Na^+ and DS^- ions with the surface charge attributed to the adsorption of DS^-, which is prescribed a surface diffusivity $D = 3.94 \times 10^{-10}$ m^2 s^{-1}, thus furnishing $Pe \approx 1.31$.

Figure 7 shows the mobilities and drag coefficients for fluid spheres (corresponding to bubbles) having small but finite $\eta_i/\eta_o = 0.01$, $\epsilon_i/\epsilon_o = 10^{-3}$ and $\kappa a = 500$. Booth's theory (dashed lines) prevails in the Debye–Hückel regime only when the kinetic-exchange rate k_d is sufficiently high. Note that increasing k_d by two orders of magnitude beyond the largest value (green lines with $k_d = 10^8$ s^{-1}) produced very little change. Schnitzer *et al.* (2014) noted Booth's theory as furnishing a mobility that vanishes as $\kappa a \to \infty$. This limit is approached very slowly, manifesting in figure 7(*a*) as a shift down the logarithmic mobility axis. Whereas the theory of Schnitzer *et al.* (2014) predicts a singular mobility at a ζ-potential that varies according to the bulk electrolyte-ion mobilities (as parameterized by their α parameter, termed a primitive Péclet number), calculations with a lower interfacial-charge mobility produced a continuous (non-singular) change in the sign of the mobility at intermediate ζ-potentials, but only with the largest values of k_d.

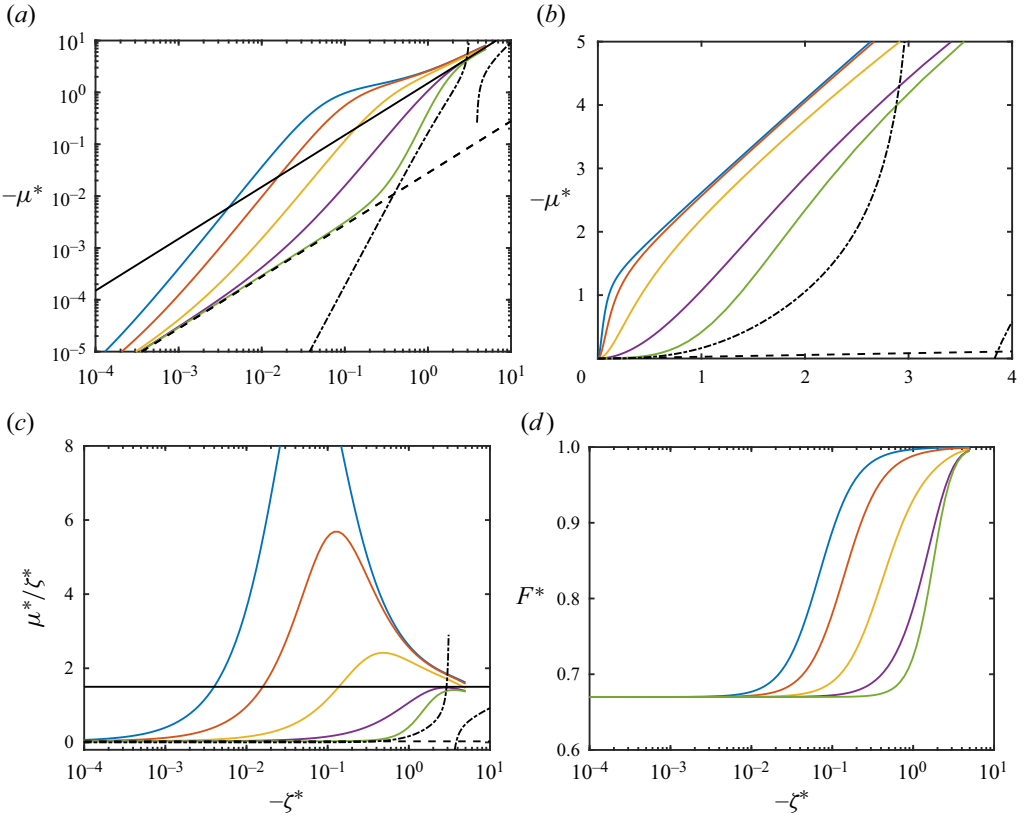

Figure 7. Scaled electrophoretic mobility $-\mu^*$ (*a*,*b*) and μ^*/ζ^* (*c*) vs $-\zeta^*$ for bubbles with a thin double layer: $\kappa a = 500$; $\eta_i/\eta_o = 0.01$; $\epsilon_i/\epsilon_o = 10^{-3}$, $k_d = 0$ (blue), 10^4, 10^5, 10^6, 10^8 (green) s^{-1}. The electrolyte comprises Na^+ and DS^- ions with $Pe_+ = u_c a/D_+ \approx 7.43 \times 10^{-4}\kappa a$ and $Pe_- = u_c a/D_- \approx 2.62 \times 10^{-3}\kappa a$, respectively, fixed ionic strength/concentration ($I = 0.1$ M) and particle radius ($a \approx 481$ nm). There is no consideration of Marangoni stresses or micellization. The surface diffusivity of the adsorbing ion (DS^-), which maintains the prescribed ζ-potential, is set to $D = 3.94 \times 10^{-10}$ m^2 s^{-1}, furnishing $Pe \approx 1.31$. Solid lines (blue through green) are computations. Solid black line in (*a*) is the Smoluchowski mobility $\mu^* = 3\zeta^*/2$ (rigid spheres, $\kappa a \gg 1$). Dashed lines in (*a–c*) are the theory of Booth (1951) ($\kappa a = 500$, $\eta_i/\eta_o = 0.01$, $\lambda = 0.5$); and the dashed-dotted lines are the theory of Schnitzer *et al.* (2014) ($\alpha = 0.5$). (*d*) Drag coefficient accompanying the mobilities in (*a–c*).

To explore further, calculations were undertaken to compare with Wu *et al.* (2021). Their computations extend Booth's model (for drops and bubbles) to higher ζ-potentials, albeit for non-conducting spheres that they termed 'dielectric' fluid droplets. In the context of the present model, this corresponds to $\epsilon_i/\epsilon_o \to 0$. Among their computations exploring the η_i/η_o and ζ^* spaces, Wu *et al.* (2021) demonstrated the mobility of highly charged, low-viscosity spheres (bubbles) as being singular when $\kappa a \approx 8$ for $\eta_i/\eta_o = 0.01$. They noted the singularity as consistent with the theory of Schnitzer *et al.* (2014), but did not address the notable disparity with the non-singular, single-signed mobilities of Baygents & Saville (1991) under similar conditions.

Wu *et al.* (2021) suggested that the singular behaviour (with a uniform surface charge) might be attributed to shortcomings of the Poisson–Boltzmann model. While this has motivated studies of finite-ion-size effects (Majhi & Bhattacharyya 2024), figure 8 demonstrates that finite interfacial-charge mobility is sufficient to regularize the

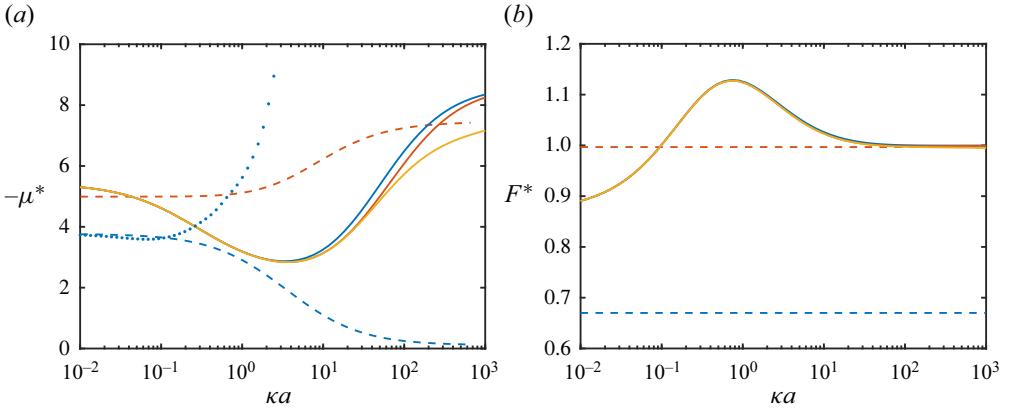

Figure 8. Scaled electrophoretic mobility μ^* (*a*) and drag coefficient F^* (*b*) vs κa for the highly charged 'dielectric' fluid spheres from figure 10 of Wu *et al.* (2021) ($\zeta^* = 5$). Mobilities from their figure 10 with $\eta_i/\eta_o = 0.01$ (dots) are singular at $\kappa a \approx 8$, transitioning to large negative values (not shown) when $\kappa \gtrsim 8$. Computations (solid lines) are undertaken with an electrolyte comprising Na^+ and DS^- ions with $\zeta^* = -5$: $k_d = 0$ (blue), 10^6 (red), 10^8 s^{-1} (yellow). Other parameters: $D = D_1 = 3.94 \times 10^{-10}$ m^2 s^{-1} (DS^-), $a = 50$ nm, $\eta_i/\eta_o = 0.01$, $\epsilon_i/\epsilon_o = 10^{-3}$. Dashed lines in (*a*) are the theory of Booth (1951) with $\lambda = 0.5$ (non-conducting drops) for $\eta_i/\eta_o = 0.01$ (blue) and 100 (red). Dashed lines in (*b*) are the Hadamard–Rybczynski drag coefficients for $\eta_i/\eta_o = 0.01$ (blue) and 100 (red).

mobility. Despite the three kinetic-exchange rates spanning eight orders of magnitude ($k_d = 0$–10^8 s^{-1}, e.g. $k_d a^2/D \approx 636$ with $k_d = 10^8$ s^{-1}), the kinetic-exchange rate is seen to have a relatively weak influence here. This reflects the high interfacial-charge density immobilizing the interface due to a strong tangential Maxwell stress. This is also evident from the large drag coefficient in panel (*b*), which is clearly enhanced by electroviscous effects ($F^* > 1$). Whereas the mobilities in figure 8 of Wu *et al.* (2021) (with slightly lower $\zeta^* = 4$) appear to grow indefinitely with κa when $\eta_i/\eta_o = 0.01$, the present model (evaluated with $\zeta^* = -4$) predicts (finite) mobilities, similar to those in figure 8, albeit shifted by approximately one dimensionless mobility unit.

3.4. *Flows, electrostatic potential and ion-concentration perturbations*

This section examines selected flow, electrostatic potential and ion-concentration perturbations underpinning the mobilities in § 3.2. These provide additional insights into the changes that finite interfacial exchange and charge mobility bring to the calculations of Baygents & Saville (1991), as highlighted in figures 4–6.

Figure 9 compares the electric-field-induced perturbations for the low- and high-viscosity drops in figure 4 with $\zeta^* = 2$ and $\kappa a = 100$. Whereas the electrostatic potential and cation-concentration perturbations are qualitatively the same (as expected based on a small Péclet number $\mathcal{P}_e \ll 1$), it should be noted that the electroosmotic flow in panel (*a*) with $\eta_i/\eta_o = 0.01$ is in the opposite direction to that in panel (*d*) with $\eta_i/\eta_o = 100$. This reflects the interface velocity for the low-viscosity drop having a large magnitude in the direction of the electrical force acting on the interfacial charge. For the high-viscosity drop, the interface is arrested by the high drop viscosity, so the electroosmotic flow at the interface is in the direction of the electrical force acting on the diffuse-layer/counter charge. Despite the local (diffuse-layer) fluid velocities in figures 9(*a*) and 9(*d*) being so different, the electrostatic potential and co-ion-concentration perturbations are similar when viewed here on the particle length scale. Much clearer

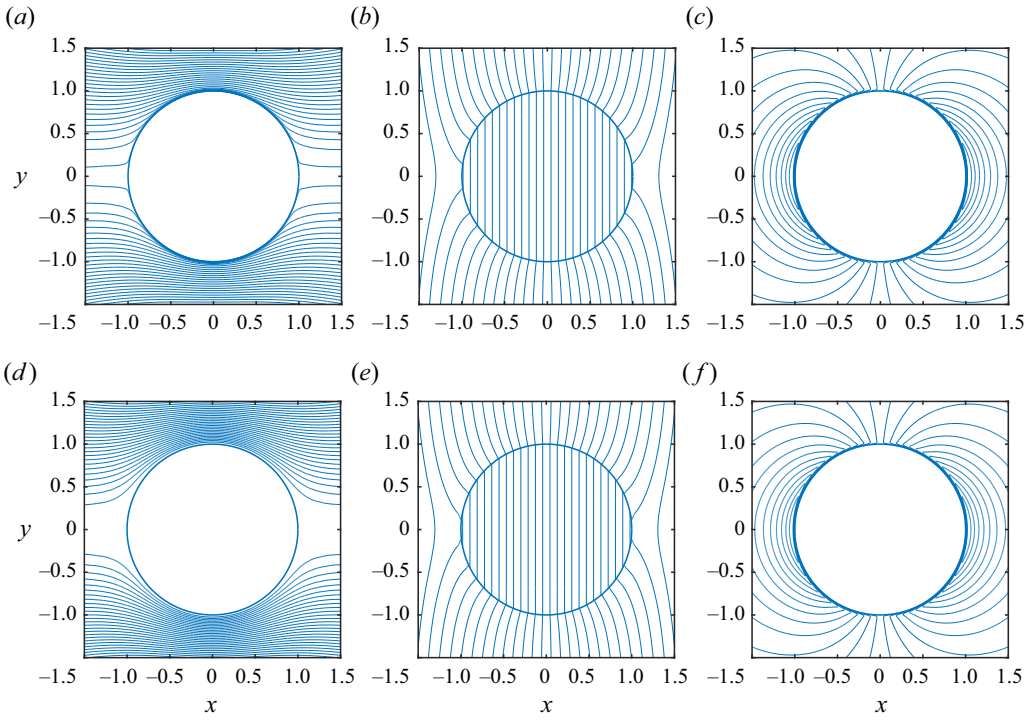

Figure 9. Streamlines (*a*,*d*), electrostatic potential perturbation (*b*,*e*) and co-cation-concentration perturbation (*c*,*f*) for stationary drops subjected to an electric field (from left to right): $\zeta^* = 2$, $\kappa a = 100$, $\eta_i/\eta_o = 0.01$ (*a*–*c*), 100 (*d*–*f*). Other parameters are the same as in figure 4. The concentration perturbations are positive (negative) at the left (right) poles.

views of perturbations within the diffuse layer are unveiled in figure 10 with $\kappa a = 1$ and ζ-potential in the Debye–Hückel regime.

Figure 11 demonstrates the flow under electrophoresis in panel (*c*) as the linear superposition of an electro-viscous flow when subjected to a uniform flow in the absence of an electric field (panel *a*) and electroosmotic flow when subjected to an electric field in the absence of translation (panel *b*). The much thicker Debye length ($\kappa a = 5$) than in figure 9 unveils qualitative features of the flows that may otherwise be absent due to the interface being arrested by the Maxwell stress (or internal viscous stresses), or completely obscured by a very small Debye length ($\kappa a \gg 1$).

Figure 12 compares the co-cation-concentration perturbations induced by translation in the absence of an electric field (*a*,*c*,*e*) with those induced by an electric field in the absence of translation (*b*,*d*,*f*). Here, the kinetic-exchange rate k_d is seen to have a significant influence on the concentration perturbation induced by the drop translation (*a*,*c*,*e*). For example, the left panel in (*a*) shows the flow-induced perturbation when there is no kinetic exchange (irreversible adsorption, $k_d = 0$). The upstream pole (flow from left to right) establishes an excess co-cation concentration, since ions from the bulk are advected into the diffuse double layer, which, at equilibrium, bears a co-cation deficit. Increasing k_d enables the adsorbed cation population to establish local equilibrium with ions in the immediately adjacent electrolyte. In panels (*e*,*f*) with $k_d = 10^5$ s^{-1}, the upstream and downstream poles now establish, respectively, a deficit and excess of co-cations (negative concentration dipole), as necessary for

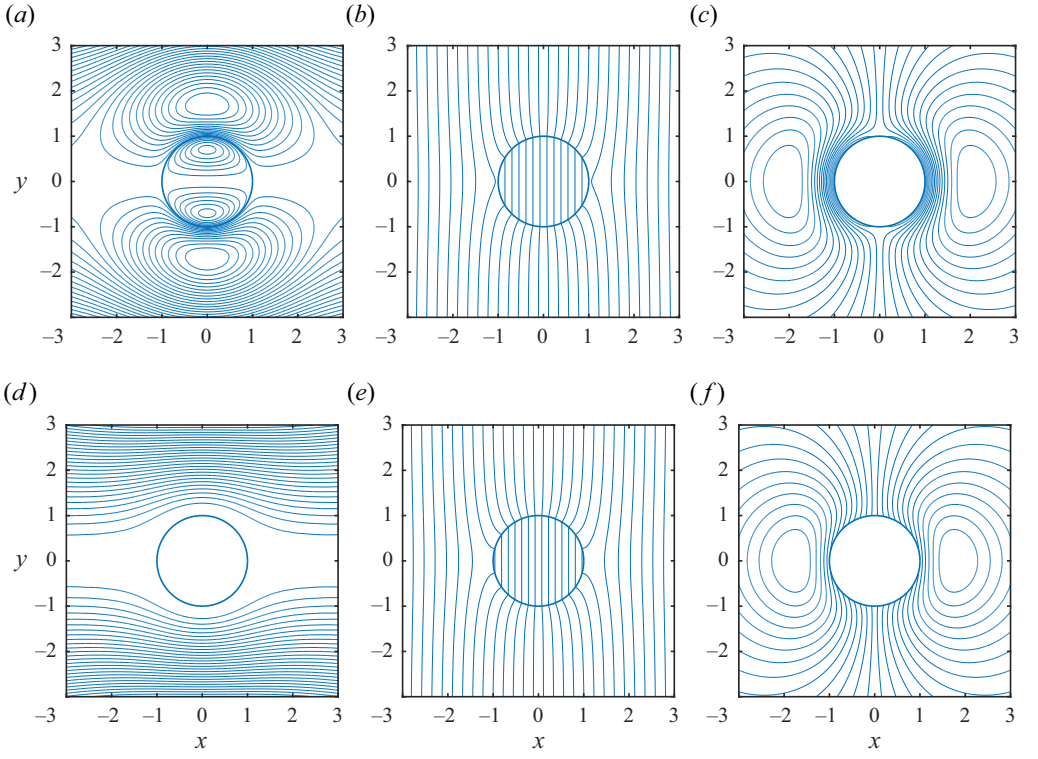

Figure 10. Streamlines (*a*,*d*), electrostatic potential perturbation (*b*,*e*) and co-cation-concentration perturbation (*c*,*f*) for stationary drops subjected to an electric field (from left to right): $\zeta^* = 0.5$, $\kappa a = 1$, $\eta_i/\eta_o = 0.01$ (*a*–*c*), 100 (*d*–*f*). Other parameters are the same as in figure 4.

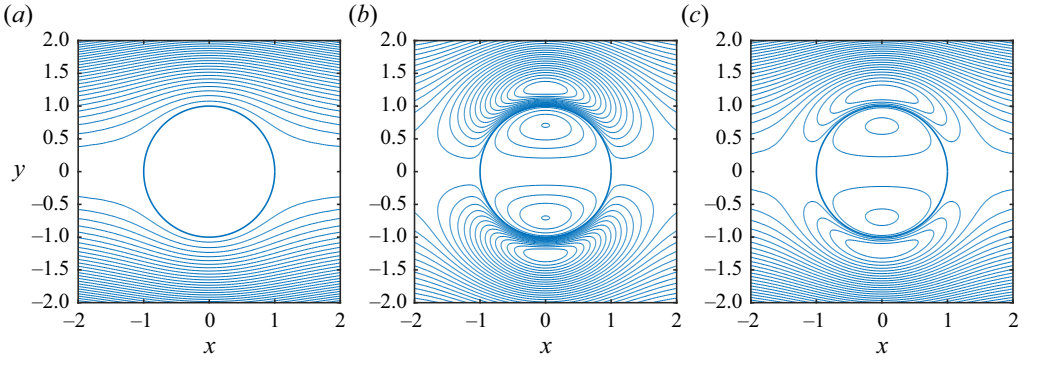

Figure 11. Streamlines (in the drop frame) for a low-viscosity drop subject to (*a*) uniform (left-to-right) far-field flow; (*b*) uniform (left-to-right) electric field; and (*c*) force-free electrophoresis: $\zeta^* = 1$, $\kappa a = 5$, $\eta_i/\eta_o = 0.01$. Other parameters are the same as in figure 4.

ions released from the downstream pole to diffuse to the upstream sink. Note that a further increase in k_d under these conditions did not further change the concentration perturbations.

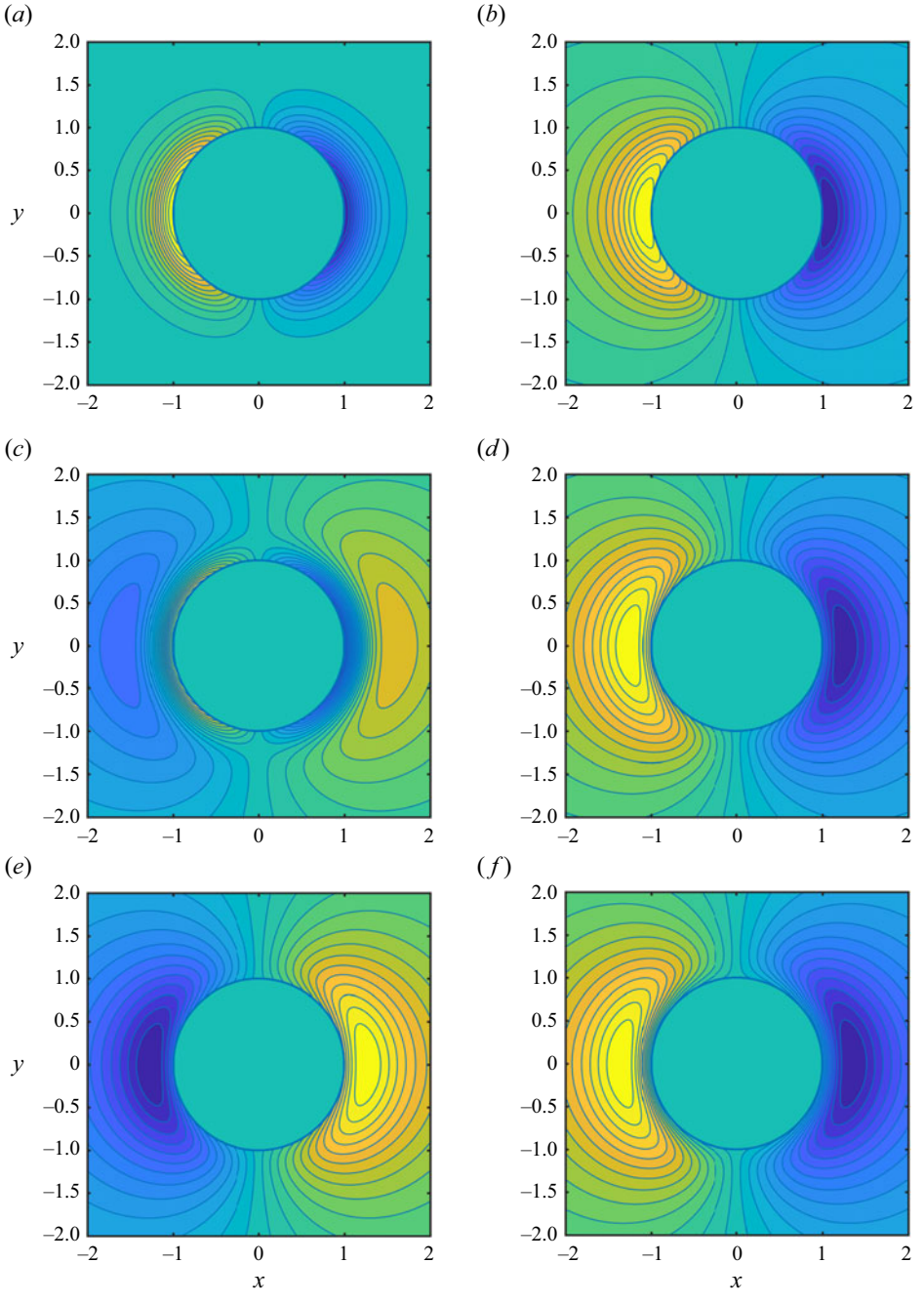

Figure 12. Co-cation-concentration perturbations (blue/negative, yellow/positive) for stationary drops subjected to a uniform (left-to-right) far-field flow (*a*,*c*,*e*) and a uniform (left-to-right) electric field (*b*,*d*,*f*): $\zeta^* = 1$, $\kappa a = 5$, $\eta_i/\eta_o = 0.01$, $k_d = 0$ (*a*,*b*), 10^4 (*c*,*d*) and 10^5 s^{-1} (*e*,*f*). Other parameters are the same as in figure 4.

3.5. *Mercury drops*

Computations were undertaken (with zero interfacial exchange, without Marangoni effects) to expedite comparisons with Ohshima *et al.* (1984) for mercury drops in KCl electrolytes. Here, however, the electrolyte is prescribed according to § 3.1, i.e. with a trace bulk concentration of the adsorbing ion. Moreover, the present model demands an extremely high dielectric permittivity for the drop to mimic how the electronic conductivity of mercury suppresses the interfacial electric field.

The results (provided in the Appendix) may be compared directly with those of Ohshima *et al.* (1984), demonstrating the mobilities (and conductivity increment) being very close to, but not exactly the same as, those of Ohshima *et al.* Drop mobilities with $|\zeta^*| \gg 1$ and $\kappa a \gg 1$ were found to be especially sensitive to the large but finite value of ϵ_i/ϵ_o: the computations reported in the Appendix were undertaken with $\epsilon_i/\epsilon_o = 10^4$, whereas the model of Ohshima *et al.* (1984) corresponds to $\epsilon_i/\epsilon_o \to \infty$. Note that correspondence is achieved with $Pe \ll 1$, thus demanding an unphysically high interfacial-charge mobility that mimics the effect a perfectly polarizable drop maintaining a perfectly uniform surface potential.

Mobilities and drag coefficients for the mercury drops of Ohshima *et al.* (1984), but with a NaCl electrolyte (zero interfacial exchange, without Marangoni effects), are shown in figure 13 for interfacial-charge mobilities furnishing $Pe \approx 0$, 0.515 and 51.5. Here, the ionic strength of the electrolyte has been adjusted to achieve the same values of κa as Ohshima *et al.* However, only the results in panel (*a*) with $Pe \approx 0$ correspond to those of Ohshima *et al.* The mobilities for drops with large ζ-potentials are lower than those computed by Ohshima *et al.* for NaCl electrolyte. This is attributed to the diffuse-layer polarization being enhanced by the lower mobility of the Na^+ counterion ion as compared with K^+; also shifting the mobility maxima to slightly larger ζ^*. Figure 13(*a*) establishes close correspondence with the thin-double-layer theory of Ohshima *et al.* (dashed lines, $\kappa a \gg 1$) when explicitly accounting for the contrasting Na^+ and Cl^- ion mobilities.

Correspondence with the thin-double-layer theory of Schnitzer *et al.* (2013) (dash-dotted lines) is demonstrated at moderate ζ-potentials and large κa by evaluating their 'primitive' ion Péclect number $\alpha = 2Pe_1Pe_2/(Pe_1 + Pe_2)$, verified here to furnish the same as the Levich–Frumkin formula provided by Ohshima *et al.* (1984). According to Schnitzer *et al.* (2013), the discrepancy at higher ζ-potentials is to be interpreted based on two asymptotically small dimensionless parameters: their theory applying when $1/(\kappa a) \ll 1$ is sufficiently smaller than $\beta = Eae/(k_BT) \ll 1$.

Whereas the consistency of the present model and the mercury-drop model of Ohshima *et al.* (1984) achieved in figure 13(*a*) occurs with a very high (unphysical) interfacial-charge mobility ($Pe \ll 1$), the drop mobilities in panels (*b*,*c*), which are notably lower, arise from much lower (and perhaps more realistic) interfacial-charge mobilities ($Pe \approx 0.515$ and $Pe \approx 51.5$). Superficially, this suggests that the correspondence with mercury drops might reflect a high surface-charge mobility maintaining a uniform concentration. However, computations (not shown) undertaken with even larger values of ϵ_i/ϵ_0 were found to bring the drop mobilities increasingly closer to those in panel (*a*). This demonstrates that the drop mobilities in panels (*b*,*c*) depart from the theory of Ohshima *et al.* (1984) due to a finite Maxwell stress acting on the interfacial charge (even though $\epsilon_i/\epsilon_o = 10^4$). Now, given that the results in figure 13 have irreversibly bound charge ($k_d = 0$), one might reasonably ask: what are the roles of interfacial exchange and charge mobility if the value of ϵ_i/ϵ_0 is even higher? To this, computations were

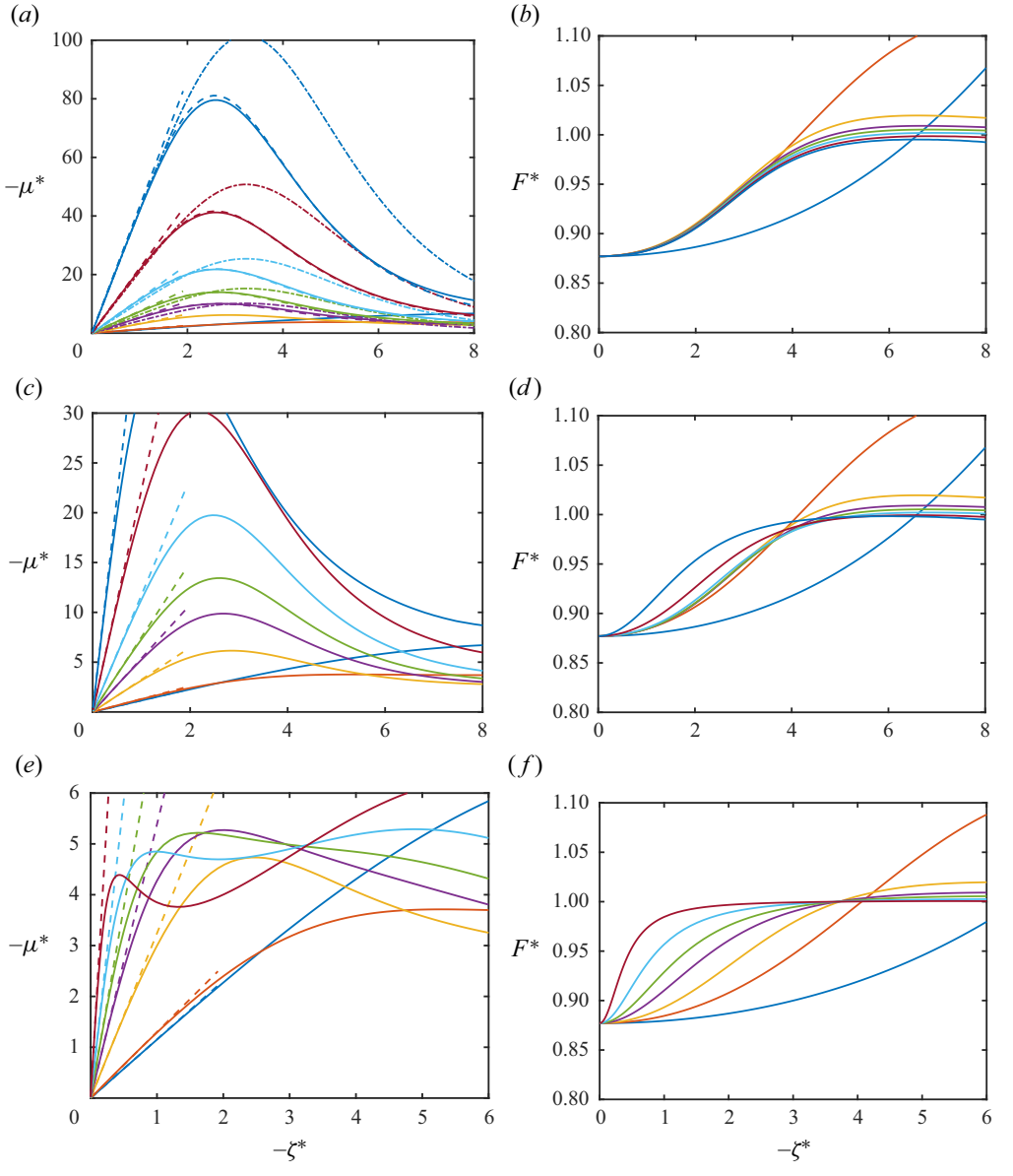

Figure 13. Scaled electrophoretic mobility $-\mu^*$ (*a*,*c*,*e*) and drag coefficient F^* (*b*,*d*,*f*) vs $-\zeta^*$ for the mercury drops of Ohshima *et al.* (1984), albeit for an aqueous NaCl electrolyte: $\kappa a = 0.1$ (blue), 1 (red), 10 (yellow), 20 (violet), 30 (green), 50 (cyan), 100 (ruby), 200 (blue). Other parameters: $k_d = 0$ (irreversibly bound charge), $Ma = 0$, $\eta_i/\eta_o = 1.71$, $\epsilon_i/\epsilon_o = 10^4$, $Pe \ll 1$ (*a*,*b*), $Pe \approx 0.515$ (*c*,*d*), $Pe \approx 51.5$ (*e*,*f*). Dashed lines in (*a*,*c*,*e*) with $|\zeta^*| \lesssim 1$ are the theoretical formula of Ohshima *et al.* (1984) in the Debye–Hückel approximation. Dashed lines in (*a*) with $\kappa a \gg 1$ are the thin-double-layer formula of Ohshima *et al.* (1984). Dashed-dotted lines in (*a*) are the thin-double-layer theory of Schnitzer *et al.* (2013) evaluated using $\alpha = 2Pe_1Pe_2/(Pe_1 + Pe_2)$, furnishing exactly the same as the Levich–Frumkin formula.

undertaken with $\epsilon_i/\epsilon_0 = 10^8$, surface diffusivity $D = 10^{-9}$ m^2 s^{-1} ($Pe = 0.515$) and $k_d = 10^8$ s^{-1}, thus furnishing $k_d a^2/D \sim 10^4$. These produced mobilities consistent with the mercury-drop model of Ohshima *et al.* (1984), demonstrating that sufficiently rapid interfacial-exchange kinetics may indeed suppress interfacial-charge density perturbations that would otherwise be sustained by interfacial advection and diffusion in the absence of interfacial electromigration.

4. Summary

This study demonstrates that interfacial kinetic exchange and interfacial-charge mobility can play a significant and perhaps under-appreciated role in fluid-sphere electrophoresis. For example, the electrophoretic mobility of dielectric fluid spheres, such as bubbles with irreversibly bound charge, is not captured by the low ζ-potential theory of Booth (1951) unless the ζ-potential is extremely small, depending on κa and the kinetic-exchange rate. This reflects in electrostatic polarization by interfacial charge and dielectric permittivity contrast. With higher interfacial charge, singular behaviour reported in the literature for low-viscosity, uniformly charged 'dielectric' spheres was regularized by the finite interfacial-charge mobility. This transformed fluid spheres (exhibiting strong internal recirculation) to their rigid-behaving counterparts. The theory of Ohshima *et al.* (1984) for mercury drops (ideally polarizable but non-ion-conducting fluid spheres) could be reproduced by prescribing a sufficiently high dielectric permittivity, irrespective of the interfacial mobility or kinetic-exchange rate. More generally, finite ζ-potentials with finite interfacial-charge mobility produce interfaces that are rigid behaving when increasing the interfacial charge, notably even in the absence of Marangoni effects, thus eliciting mobilities of rigid spheres that are indifferent to the dielectric permittivity contrast, as expected from the standard electrokinetic model (O'Brien & White 1978). This paper has sought to identify pertinent features of a model that must ultimately be applied to interpret specific fluid-sphere systems, albeit within the weak-field approximation. An exploration of how this model might provide a unified interpretation of ζ-potentials from experimental studies of micro- and nano-bubbles will be reported elsewhere.

Funding. This research (initiated during a sabbatical leave in 2020) was supported by an NSERC Discovery grant. The author is grateful to Proferssor E. Yariv (Technion, Israel University of Technology) for sharing his insights on the electrophoresis of large spherical bubbles during the preparation of this manuscript.

Declaration of interests. The author reports no conflict of interest.

Author ORCIDs.
Reghan J. Hill https://orcid.org/0000-0001-9735-0389.

Appendix. Mercury drops with KCl electrolyte, as computed by Ohshima *et al.* (1984)

The results in figure 14 were computed with the same electrolyte and other model parameters as Ohshima *et al.* (1984) (for $\epsilon_i/\epsilon_o = \infty$), provided here as a partial validation of the computational solution of the model developed in the main text, implemented here with zero interfacial exchange ($k_d = 0$), without Marangoni effects ($Ma = 0$). The reciprocal drag coefficient $1/F^*$ is equivalent to the reduced sedimentation velocity of Ohshima *et al.*

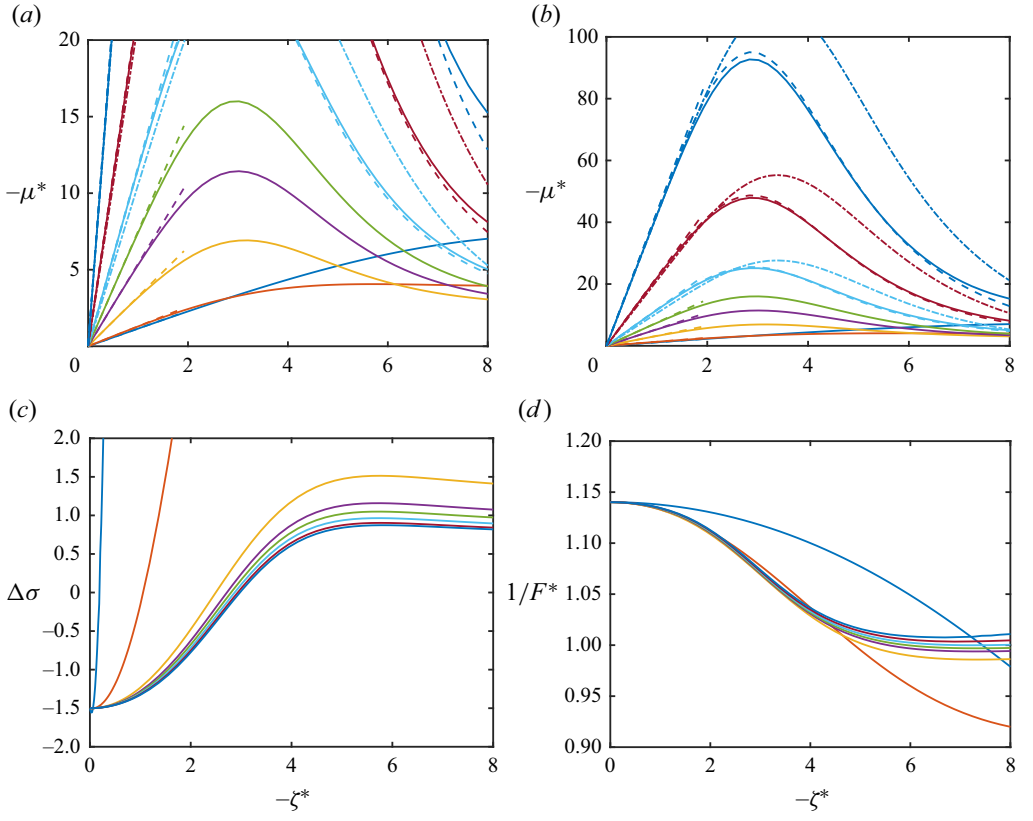

Figure 14. Scaled electrophoretic mobility $-\mu^*$ (*a*,*b*), conductivity increment $\Delta\sigma$ (*c*) and sedimentation velocity $1/F^*$ (*d*) vs $-\zeta^*$ for the mercury drops of Ohshima *et al.* (1984) (aqueous KCl electrolyte): $\kappa a = 0.1$ (blue), 1 (red), 10 (yellow), 20 (violet), 30 (green), 50 (cyan), 100 (ruby), 200 (blue). Other parameters: $k_d = 0$ (irreversibly bound charge), $Ma = 0$, $\eta_i/\eta_o = 1.71$, $\epsilon_i/\epsilon_o = 10^4$, $Pe \ll 1$. Dashed lines in (*a*,*b*) are the theoretical formulas of Ohshima *et al.* (1984) for $\zeta^* \lesssim 1$ and $\kappa a \gg 1$ (non-ion-conducting fluid spheres). Dashed-dotted lines in (*a*,*b*) are the thin-double-layer theory of Schnitzer *et al.* (2013) with $\alpha = 2Pe_1Pe_2/(Pe_1 + Pe_2)$, furnishing exactly the same as the Levich–Frumkin formula.

References

Adams, J.E., Brown, R.S. & Hodson, P.V. 2020 The bioavailability of oil droplets trapped in river gravel by hyporheic flows. *Environ. Pollut.* **269**, 116110.

Alty, T. 1924 The cataphoresis of gas bubbles in water. *Proc. R. Soc. Lond.* A **106** (737), 315–340.

Atamanchuk, D., Koelling, J., Send, U. & Wallace, D.W.R. 2020 Rapid transfer of oxygen to the deep ocean mediated by bubbles. *Nat. Geosci.* **13**, 232–237.

Baygents, J.C. & Saville, D.A. 1991 Electrophoresis of drops and bubbles. *J. Chem. Soc. Faraday Trans.* **87** (12), 1883–1898.

Booth, F. 1951 The cataphoresis of spherical fluid droplets in electrolytes. *J. Chem. Phys.* **19** (11), 1331–1336.

Borden, M.A., Shakya, G., Upadhyay, A. & Song, K.-H. 2020 Acoustic nanodrops for biomedical applications. *Curr. Opin. Colloid Interface Sci.* **50**, 101383.

Hill, R.J. 2020 Electrokinetic spectra of dilute surfactant-stabilized nano-emulsions. *J. Fluid Mech.* **902**, A15.

Hill, R.J. & Afuwape, G. 2020 Dynamic mobility of surfactant stabilized nano-drops: unifying equilibrium thermodynamics, electro-kinetics and Marangoni effects. *J. Fluid Mech.* **895**, A14.

Hill, R.J., Saville, D.A. & Russel, W.B. 2003 Electrophoresis of spherical polymer-coated colloidal particles. *J. Colloid Interface Sci.* **258** (1), 56–74.

HO, T.M., RAZZAGHIC, A., RAMACHANDRANC, A. & MIKKONEN, K.S. 2022 Emulsion characterization via microfluidic devices: a review on interfacial tension and stability to coalescence. *Adv. Colloid Interface Sci.* **299**, 102541.

JIN, J., FENG, Z., YANG, F. & GU, N. 2019 Bulk nanobubbles fabricated by repeated compression of microbubbles. *Langmuir* **35**, 4238–4245.

KELSALL, G.H., TANG, S., YURDAKULT, S. & SMITH, A.L. 1996 Electrophoretic behaviour of bubbles in aqueous electrolytes. *J. Chem. Soc. Faraday Trans.* **92** (20), 3887–3893.

LYU, T., WU, S., MORTIMER, R.J.G. & PAN, G. 2019 Nanobubble technology in environmental engineering: revolutionization potential and challenges. *Environ. Sci. Technol.* **53**, 7175–7176.

MAHAPATRA, P., OHSHIMA, H. & GOPMANDAL, P.P. 2022 Electrophoresis of dielectric and hydrophobic spherical fluid droplets possessing uniform surface charge density. *Langmuir* **38**, 11421–11431.

MAJHI, S. & BHATTACHARYYA, S. 2024 Finite ion size effects on electrophoresis of a dielectric surfactant-laden droplet in a non-dilute electrolyte. *Appl. Math. Mod.* **132**, 384–401.

NIRMALKAR, N., PACEK, A.W. & BARIGOU, M. 2018 Interpreting the interfacial and colloidal stability of bulk nanobubbles. *Soft Matt.* **14**, 9643.

O'BRIEN, R.W. & WHITE, L.R. 1978 Electrophoretic mobility of a spherical colloidal particle. *J. Chem. Soc. Faraday Trans.* **74**, 1607–1626.

OHSHIMA, H., HEALY, T.W. & WHITE, L.R. 1984 Electrokinetic phenomena in a dilute suspension of charged mercury drops. *J. Chem. Soc. Faraday Trans.* **80** (12), 1643–1667.

PULLANCHERY, S., KULIK, S., OKUR, H.I., DE AGUIAR, H.B. & ROKE, S. 2020 On the stability and necessary electrophoretic mobility of bare oil nanodroplets in water. *J. Chem. Phys.* **152**, 241104.

RUSSEL, W.B., SAVILLE, D.A. & SHOWALTER, W.R. 1989 *Colloidal Dispersions*. Cambridge University Press.

SCHNITZER, O., FRANKEL, I. & YARIV, E. 2013 Electrokinetic flows about conducting drops. *J. Fluid Mech.* **722**, 394–423.

SCHNITZER, O., FRANKEL, I. & YARIV, E. 2014 Electrophoresis of bubbles. *J. Fluid Mech.* **753**, 49–79.

TAKAHASHI, M. 2005 ζ-potential of microbubbles in aqueous solutions: electrical properties of the gas-water interface. *J. Phys. Chem.* B **109**, 21858–21864.

TSAI, M.-Y., FAN, L., TSENG, J., LIN, J., TSENG, A. & LEE, E. 2022 Electrophoresis of a highly charged fluid droplet in dilute electrolyte solutions: analytical Hückel-type solution. *Electrophoresis* **43** (15), 1611–1616.

TSENG, J., SU, J., CHANG, K., CHANG, A., CHUANG, L., LU, A., LEE, R. & LEE, E. 2023 Electrophoresis of a dielectric droplet with constant surface charge density. *Electrophoresis* **44**, 1810–1817.

USHIKUBOA, F.Y., FURUKAWAA, A., NAKAGAWAA, R., ENARIA, M., MAKINOA, Y., KAWAGOEA, Y., SHIINAB, T. & OSHITA, S. 2010 Evidence of the existence and the stability of nano-bubbles in water. *Colloids Surf. (*A*)* **361**, 31–37.

USUI, S., SASAKI, H. & MATSUKAWA, H. 1981 The dependence of zeta potential on bubble size as determined by the Dorn effect. *J. Colloid Interface Sci.* **81** (1), 80–84.

WHYBREW, W.E., KINZER, G.D. & GUNN, R. 1952 Electrification of small air bubbles in water. *J. Geophys. Res.* **57** (4), 459–471.

WU, Y., FAN, L., JIAN, E. & LEE, E. 2021 Electrophoresis of a highly charged dielectric fluid droplet in electrolyte solutions. *J. Colloid Interface Sci.* **598**, 358–368.

YANG, C., DABROS, T., LI, D., CZARNECKI, J. & MASLIYAH, J.H. 2001 Measurement of the zeta potential of gas bubbles in aqueous solutions by microelectrophoresis method. *J. Colloid Interface Sci.* **243**, 128–135.

ZHANG, H., GUO, Z. & ZHANG, X. 2020 Surface enrichment of ions leads to the stability of bulk nanobubbles. *Soft Matt.* **16**, 5470.

ZHU, J., AN, H., ALSHEBRI, M., LIU, L., TERPSTRA, P.M.J., LIU, G. & CRAIG, V.S.J. 2016 Cleaning with bulk nanobubbles. *Langmuir* **32** (43), 11203–11211.

ZUKOSKI, C.F. & SAVILLE, D.A. 1986 The interpretation of electrokinetic measurements using a dynamic model of the Stern layer: I. The dynamic model. *J. Colloid Interface Sci.* **114** (1), 32–44.